Studies in Applied Mathematics

WILEY

STUDIES IN APPLIED MATHEMATICS

ORIGINAL ARTICLE OPEN ACCESS

A Multiparameter Singular Perturbation Analysis of the Robertson Model

Lukas Baumgartner | Peter Szmolyan

Institute of Analysis and Scientific Computing, TU Wien, Vienna, Austria

Correspondence: Lukas Baumgartner (lukas.baumgartner@tuwien.ac.at)

Received: 7 August 2024 | **Revised:** 10 January 2025 | **Accepted:** 22 January 2025

Funding: This study was supported by Technische Universität Wien.

Keywords: blowup method | geometric singular perturbation theory | multiparameter singular perturbation | Robertson model

ABSTRACT

The Robertson model describing a chemical reaction involving three reactants is one of the classical examples of stiffness in ODEs. The stiffness is caused by the occurrence of three reaction rates k_1, k_2, and k_3, with largely differing orders of magnitude, acting as parameters. The model has been widely used as a numerical test problem. Surprisingly, no asymptotic analysis of this multiscale problem seems to exist. In this paper, we provide a full asymptotic analysis of the Robertson model under the assumption $k_1, k_3 \ll k_2$. We rewrite the equations as a two-parameter singular perturbation problem in the rescaled small parameters $(\varepsilon_1, \varepsilon_2) := (k_1/k_2, k_3/k_2)$, which we then analyze using geometric singular perturbation theory (GSPT). To deal with the multiparameter singular structure, we perform blowups in parameter- and variable space. We identify four distinct regimes in a neighborhood of the singular limit $(\varepsilon_1, \varepsilon_2) = (0, 0)$. Within these four regimes, we use GSPT and additional blowups to analyze the dynamics and the structure of solutions. Our asymptotic results are in excellent qualitative and quantitative agreement with the numerics.

MSC2020: 34E10, 34E13, 34E15, 92E20

1 | Introduction

In this paper, we give a dynamical systems analysis of the Robertson model [30] based on methods from geometric singular perturbation theory (GSPT). The Robertson model describes a chemical reaction of three reactants X, Y, and Z, which interact according to the reaction scheme shown in Figure 1.

With mass-action kinetics, the Robertson model leads to the following system of ODEs:

$$\begin{aligned} \dot{x} &= -k_1 x + k_3 yz \\ \dot{y} &= k_1 x - k_2 y^2 - k_3 yz \\ \dot{z} &= k_2 y^2, \end{aligned} \tag{1.1}$$

with corresponding concentrations $x, y, z \in \mathbb{R}$, reaction rates $k_i > 0, i = 1, 2, 3$. As usual, $(\dot{\ }) := \frac{d}{dt}$ denotes the time derivative. The classical choice of parameters and initial values in [30] is

$$k_1 = 4 \cdot 10^{-2}, \quad k_2 = 3 \cdot 10^7, \quad k_3 = 10^4 \tag{1.2}$$

and

$$(x(0), y(0), z(0))^T = (1, 0, 0)^T. \tag{1.3}$$

The qualitative dynamics of system (1.1) is fairly simple.

Lemma 1.1. *All solutions of (1.1) starting in the nonnegative orthant $\mathbb{R}^3_+$ exist globally in forward time. The z-axis is a line of attracting equilibria. The solution with initial value $(x_0, y_0, z_0)^T \in$*

$$
\begin{array}{ccc}
X & \xrightarrow{K_1} & Y \\
Y+Y & \xrightarrow{K_2} & Y+Z \\
Y+Z & \xrightarrow{K_3} & X+Z
\end{array}
$$

FIGURE 1 | Reaction scheme of the Robertson model.

$\mathbb{R}^3_+$ *converges to the equilibrium* $(\hat{x}, \hat{y}, \hat{z})^T = (0, 0, c)^T$, *with* $c := x_0 + y_0 + z_0 > 0$.

Proof. Adding the three equations of (1.1) implies that the quantity $x + y + z = const.$ is conserved. Since on the boundary of the nonnegative orthant $\mathbb{R}^3_+$, the flow does not point outward, that is,

$$\dot{x}|_{x=0} = k_3 yz \geq 0, \quad \dot{y}|_{y=0} = k_1 x \geq 0, \quad \dot{z}|_{z=0} = k_2 y^2 \geq 0,$$

we can conclude that $\mathbb{R}^3_+$ is forward invariant under (1.1), see [1, p. 219]. Consequently, the solution starting at an initial value $(x_0, y_0, z_0)^T \in \mathbb{R}^3_+$, where $0 < c := x_0 + y_0 + z_0$, is contained in the compact set

$$K = \left\{ (x, y, z)^T \in \mathbb{R}^3_+ \,:\, x + y + z = c \right\}$$

and therefore exists for all times $t \geq 0$.

Due to the conserved quantity, we may reduce the dimension of (1.1) by using $x = c - y - z$ to obtain

$$
\begin{aligned}
\dot{y} &= k_1(c - y - z) - k_2 y^2 - k_3 yz \\
\dot{z} &= k_2 y^2.
\end{aligned}
\tag{1.4}
$$

Since the divergence of the vector field (1.4) given by $-k_1 - 2k_2 y - k_3 z$ is negative for positive reaction rates, we can exclude nonconstant periodic solutions by the Bendixson–Dulac criterion. The unique equilibrium of (1.4) is given by $(\hat{y}, \hat{z})^T = (0, c)^T$, hence by the Poincaré–Bendixson theorem all solutions of (1.4) will ultimately converge to this equilibrium. □

In particular, we conclude from Lemma 1.1 that the solution of (1.1) with initial value (1.3) converges to the unique equilibrium $(\hat{x}, \hat{y}, \hat{z})^T = (0, 0, 1)^T$. Thus, our interest in the Robertson model is not this rather simple dynamics but the multiscale structure of these solutions which we now describe in a preliminary way based on numerical simulations. The time series of a numerical solution of (1.1) with the classical choice of reaction rates (1.2) and initial condition (1.3) is shown in Figure 2.

In the time series, three distinct parts can be distinguished. The reaction starts with a very fast initial increase of y up to a plateau value $y^{max}_{num} \approx 3.65 \cdot 10^{-5}$. This is followed by an intermediate phase where y is almost constant. In the third part, the conversion of x into z (via y) proceeds on a much longer time scale.

Remark 1.2. Our analysis predicts a plateau value of $y^{max} = \sqrt{\frac{k_1 c}{k_2}} + \mathcal{O}(\frac{k_1}{k_2})$. A detailed derivation of this value can be found at the end of Section 3. With the parameter values (1.2) and initial condition (1.3) (which implies $c = 1$) this leads to $y^{max} = \frac{2}{\sqrt{3}} \cdot 10^{-\frac{9}{2}} + \mathcal{O}(10^{-9}) = 3.651 \cdot 10^{-5} + \mathcal{O}(10^{-9})$, which matches the numerical value y^{max}_{num} above.

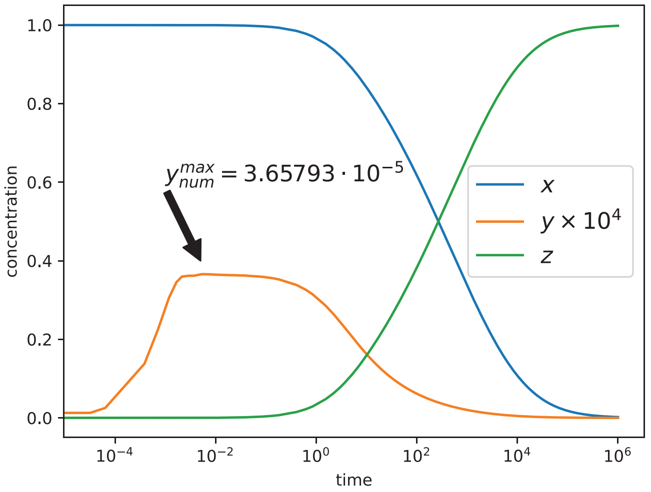

FIGURE 2 | Numerical solution of Equation (1.1) with an implicit BDF solver [32]. Note the logarithmic time scale.

Numerical experiments indicate that this solution structure occurs for all parameter values

$$0 < k_1, k_3 \ll k_2. \tag{1.5}$$

This peculiar structure of solutions has been observed early on as the Robertson model was widely used as a test problem for stiff numerical solvers, for example, [14, p. 3]. Up to our knowledge, the Robertson model (1.1) has been investigated only numerically. No analytical results explaining the solution structure described above seem to be available. In this paper, we provide a full asymptotic analysis of the Robertson model under the assumption $k_1, k_3 \ll k_2$, which covers the classical values (1.2). We rewrite the equations as a two-parameter singular perturbation problem in the rescaled small parameters $(\varepsilon_1, \varepsilon_2) := (k_1/k_2, k_3/k_2)$, which we then analyze using GSPT.

Similar phenomena and solution structures occur in many chemical reactions and more general classes of biological models. Due to the occurrence of variables and parameters of widely different orders of magnitude most of these models are multiscale in nature, see, for example, [22, 33, 34] and references therein. As a consequence of these multiple scales, some variables may vary little and can thus be treated as constants. Some parameters may have almost no effect and can be neglected. Some variables may rapidly approach a (quasi)equilibrium and can thus be slaved to other variables. Different mechanisms may dominate the dynamics in certain regions of phase- and/or parameter-space. Correspondingly, individual trajectories contain segments generated by sequences of fast and slow processes on widely separated time scales. Identifying and analyzing these regimes and the resulting decompositions into subsystems is crucial in the analysis of the dynamics. In suitably scaled variables, the equations in the individual regimes often have the form of a slow–fast dynamical system and the dynamics is (locally) organized by a slow invariant manifold of lower dimension. The dynamics on the slow manifold is governed by a reduced model of lower dimension.

The most widely used realization of these ideas is the well-known quasi-steady-state approximation (QSSA), which is used to obtain lower-dimensional approximating models, that is, reactants involved in fast processes are eliminated by assuming that they are in equilibrium [33, 34].

A powerful mathematical concept in explaining these phenomena are slow manifolds. The mathematical theory of slow manifolds and more general of slow–fast dynamical systems, known as GSPT, is well-developed for ODEs depending singularly on one distinguished parameter $\varepsilon \ll 1$ (see [10, 19, 24, 27, 38] an the numerous references therein). The origins of GSPT date back to the work of Fenichel [10], where he introduced an invariant manifold approach for singularly perturbed differential equations of the form

$$z' = H(z, \varepsilon) \tag{1.6}$$

with $z \in \mathbb{R}^k$, $k \geq 2$, and $\varepsilon \ll 1$, see also [38] for a modern presentation. In this setting, singular perturbation problems correspond to situations where the set

$$\mathcal{S} := \{z \in \mathbb{R}^k : H(z, 0) = 0\}$$

contains manifolds of dimension $l \geq 1$. In many situations, $\mathcal{S}$ is a manifold of dimension l, however, in other situations it is not a manifold in the strict sense due to the existence of singular points. Therefore, $\mathcal{S}$ is denoted as the critical set. The critical set $\mathcal{S}$ corresponds to the equilibrium points of the $\varepsilon = 0$ limit of (1.6) $z' = H(z, 0)$. Under certain conditions, manifolds $\tilde{\mathcal{S}} \subset \mathcal{S}$ perturb to slow manifolds $\tilde{\mathcal{S}}_\varepsilon$ for $0 < \varepsilon \ll 1$ on which the dynamics is slow, while away from $\tilde{\mathcal{S}}_\varepsilon$ the dynamics is fast.

An important special case of (1.6) are slow–fast systems in standard form given by

$$\begin{aligned} x' &= f(x, y, \varepsilon) \\ y' &= \varepsilon g(x, y, \varepsilon) \end{aligned} \tag{1.7}$$

with $x \in \mathbb{R}^m$, $y \in \mathbb{R}^n$, and $\varepsilon \ll 1$, where differentiation is with respect to the fast time τ. Systems of the form (1.7) are called slow–fast in standard form, because as long as f and g are $\mathcal{O}(1)$ the dynamics of x is fast compared to y, that is, x is the fast variable and y the slow variable.

Remark 1.3. It will turn out that for the analysis of the Robertson model both forms (1.6) and (1.7) are relevant. In the following explanation of the basic principles of GSPT, we will limit ourselves to the important special case (1.7).

The $\varepsilon = 0$ limit problem of (1.7)

$$\begin{aligned} x' &= f(x, y, 0) \\ y' &= 0 \end{aligned} \tag{1.8}$$

is called *layer problem*, which is used as an approximation of the fast dynamics. With a slight abuse of notation, we denote the set of equilibria of (1.8)

$$\mathcal{S} = \left\{(x, y)^T \in \mathbb{R}^{m+n} : f(x, y, 0) = 0\right\},$$

as *critical manifold*, despite the fact that $\mathcal{S}$ does not need to be a manifold in the strict sense (as pointed out above in the discussion of the general form (1.6)). By switching to the slow time $t = \varepsilon\tau$, we may write system (1.7) in the (for $\varepsilon > 0$) equivalent form

$$\begin{aligned} \varepsilon\dot{x} &= f(x, y, \varepsilon) \\ \dot{y} &= g(x, y, \varepsilon), \end{aligned} \tag{1.9}$$

where differentiation is with respect to the slow time t. The limit problem on the slow time scale

$$\begin{aligned} 0 &= f(x, y, 0) \\ \dot{y} &= g(x, y, 0) \end{aligned} \tag{1.10}$$

is called *reduced problem* and is used as an approximation of the slow dynamics. Observe that the reduced problem is a dynamical system on the critical manifold $\mathcal{S}$. Parts of the critical manifold $\mathcal{S}$, where the Jacobian $\frac{\partial f}{\partial x}$ is regular, may be represented locally as graphs $x = h(y)$ by the implicit function theorem. The reduced flow on $\mathcal{S}$ is then given by

$$\dot{y} = g(h(y), y, 0).$$

The goal of GSPT is to combine the dynamics of the two simpler limiting systems (1.8), and (1.10) to understand the behavior of (1.7) for $0 < \varepsilon \ll 1$. In [10], Fenichel showed that if the Jacobian $\partial_x f$ is uniformly hyperbolic, the critical manifold $\mathcal{S}$ perturbs smoothly to a locally invariant slow manifold $\mathcal{S}_\varepsilon$ which is $\mathcal{O}(\varepsilon)$-close to $\mathcal{S}$, shares its stability properties with $\mathcal{S}$ and the slow flow on $\mathcal{S}_\varepsilon$ converges to the reduced flow as $\varepsilon \to 0$.

A major difficulty that remained in GSPT were nonhyperbolic points, that is, points where at least one eigenvalue of the Jacobian $\partial_x f$ lies on the imaginary axis. Frequently, these points are given by the singularities of the critical manifold. The problem remained open until the pioneering work of Dumortier and Roussarie [9] where they introduced the blowup method, which was then developed into a powerful tool in GSPT by Krupa and Szmolyan, see [24, 25]. The main idea of the blowup method is to first extend the state space by adding the trivial equation $\varepsilon' = 0$ and then introducing suitable weighted spherical coordinates to blow up the singularity, for example, a point to a sphere or a line to a cylinder. After dividing out a suitable power of the radial variable, less singular differential equations are obtained which often allow for a complete analysis with dynamical systems tools. By now, the blowup method has been widely used in the analysis of singularly perturbed differential equations (see, e.g. [6, 13, 15, 16, 20, 21, 26, 29, 35]). It seems fair to say that GSPT is very well developed for systems with a distinguished singular perturbation parameter ε and that it has proven to be very useful in a large array of applications.

However, surprisingly little seems to be known in the case of systems depending singularly on several small or large parameters, for example, chemical reactions with reaction rates

k_i, $i = 1, \dots, p$ of widely differing orders of magnitude. Since this singular dependence on several parameters is rather the rule than the exception for realistic chemical reactions and many other classes of biological models, it is important to develop methods suitable for the asymptotic analysis of such problems.

Our interest in the Robertson model comes from the fact, that it is a well-known but fairly simple representative of this class of problems. We expect that the approach of this paper will be useful in a wide variety of problems, for example, various variants and extensions of the basic Michaelis–Menten mechanism [11, 31] and models of the Belousov–Zhabotinskii reaction [37]. In ongoing work, we are using this approach in the analysis of a five-variable model of the cell cycle [8, 36] with singular dependence on three parameters.

An obvious and often used approach to apply asymptotic methods and in particular GSPT to multiparameter problems is to reduce to the one-parameter case by identifying a suitable parameter ε such that

$$(k_1, \dots, k_p)^T \sim (\varepsilon^{\alpha_1}, \dots, \varepsilon^{\alpha_p})^T,\ \alpha_i \in \mathbb{Z},\ i = 1, \dots, p. \tag{1.11}$$

A simple illustration of this approach (and its inherent arbitrariness) in the context of the Robertson model with the classical parameters (1.2) would be $\varepsilon = 1/10$ which leads to $\alpha_1 = 2$, $\alpha_2 = -7$, and $\alpha_3 = -4$. This widely used approach, where parameters are restricted to a curve, can be very successful if good numerical values of the parameters are available (see, e.g., [18, 22]). Unfortunately, this is often not the case and tools for qualitative analysis covering wider ranges of parameters are needed.

A powerful tool in finding significant scalings of parameters and variables in (polynomial) systems of differential equations based on Newton polyhedra and the associated power transformations was developed by Bruno (see [3] and references therein). A related approach based on ideas from tropical geometry has been developed in [8, 22]. The connections between these approaches and our geometric approach will be explored in future work. Clearly, such problems can also be treated by more conventional methods based on matched asymptotic expansions. An advantage of the geometric dynamical systems approach is that it provides (i) detailed insight into the underlying singular structures and (ii) leads to rigorous results on the dynamics in appropriate ranges of the parameters.

Hence, it is desirable to develop or adapt GSPT to problems depending singularly on several independent parameters $(\varepsilon_1, \dots, \varepsilon_l)^T$, $l \geq 2$. Such problems are potentially more challenging since the singular behavior and the multiscale structure can vary significantly in a neighborhood of the singular limit $(\varepsilon_1, \dots, \varepsilon_l)^T = (0, \dots, 0)^T$. As a step toward a framework for multiparameter singular perturbations of ODEs, we distinguish three different cases. We expect that this classification is preliminary and not exhaustive, nevertheless we feel it is useful as a first step. For simplicity, we phrase this classification for systems depending on two parameters, but it can be easily extended to systems depending on more parameters.

Case 1: There exists an ordered sequence of time scales, that is, the system of differential equations has the form

$$\begin{aligned} \dot{x}_1 &= f_1(x, \varepsilon_1, \varepsilon_2) \\ \dot{x}_2 &= \varepsilon_1 f_2(x, \varepsilon_1, \varepsilon_2) \\ \dot{x}_3 &= \varepsilon_1 \varepsilon_2 f_3(x, \varepsilon_1, \varepsilon_2), \end{aligned} \tag{1.12}$$

with $0 < \varepsilon_1, \varepsilon_2 \ll 1$, which is the three-time scale analog to the slow–fast standard form (1.7). In this situation, one can apply Fenichel theory iteratively to obtain a nested sequence of critical manifolds. This case is fairly well understood if the manifolds are normally hyperbolic (see [4]). If there are nonhyperbolic points, the situation can be more complicated, for example, see the early influential paper [23] and the more recent [17].

In the two remaining cases, we consider more general systems in nonstandard form, that is,

$$\dot{z} = H(z, \varepsilon_1, \varepsilon_2) \tag{1.13}$$

with $0 < \varepsilon_1, \varepsilon_2 \ll 1$.

Case 2: The parameter ε_1 is a classical singular perturbation parameter of (1.13) with corresponding critical manifold $\mathcal{S}(\varepsilon_2)$ (depending on ε_2) by standard Fenichel theory. The singular dependence of (1.13) on ε_2 is caused by singularities of the critical manifold $\mathcal{S}(\varepsilon_2)$ as $\varepsilon_2 \to 0$, for example, $\mathcal{S}(\varepsilon_2)$ loses normal hyperbolicity (see [15, 21]).

Case 3: Both parameters ε_1 and ε_2 act as singular perturbation parameters, leading to fundamentally different slow–fast structures in different regions of the parameter space.

So far, the analysis of problems corresponding to cases 2 and 3 has been carried out mostly in the form of individual case studies, for example, see the very interesting work [7] and also [5]. For more examples and an attempt to extract common features of existing results, we refer to the recent review [28] and the many references therein.

The goal of this work is to make progress on adapting and extending GSPT to multiparameter singular perturbation problems which is the topic of the ongoing thesis project [2]. We give an asymptotic analysis of the Robertson model (1.1) under the assumption (1.5), which covers the classical choice (1.2) in [30]. It turns out that the Robertson model has features of cases 2 and 3, which shows that the above classification is not strict. We view our analysis as a step in adapting GSPT to multiparameter singular perturbation problems like (1.13) and also as a starting point for the analysis of similar problems depending on more than two parameters. First, we rewrite (1.1) as a two-parameter singular perturbation problem in the rescaled parameters

$$(\varepsilon_1, \varepsilon_2)^T := (k_1/k_2, k_3/k_2)^T \in \mathbb{R}_+ \times \mathbb{R}_+$$

varying in a neighborhood of $(\varepsilon_1, \varepsilon_2)^T = (0, 0)^T$.

Recall from the proof of Lemma 1.1, that we can reduce the Robertson model to a planar dynamical system of the form (1.4).

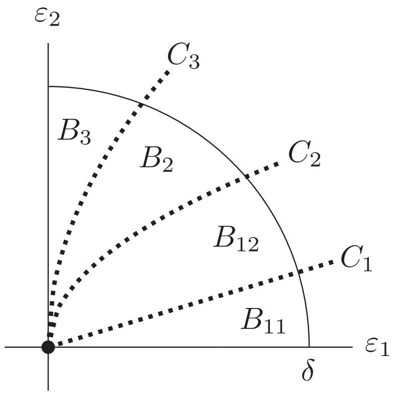

FIGURE 3 | The four scaling regions B_{11}, B_{12}, B_2, and B_3.

By switching to the fast time scale $\tau = k_2 t$, we obtain

$$\begin{aligned} y' &= \varepsilon_1(c - y - z) - y^2 - \varepsilon_2 yz \\ z' &= y^2, \end{aligned} \tag{1.14}$$

with initial value $(y_0, z_0)^T = (0,0)^T$, " ′ " denotes the derivative with respect to the fast time τ, and $0 < \varepsilon_1, \varepsilon_2 \ll 1$. System (1.14) is now a planar multiparameter singularly perturbed differential equation of the form (1.13). Up to a reparameterization of time, system (1.14) is equivalent to (1.1), hence, we will perform our GSPT analysis based on the planar system (1.14).

Remark 1.4. It follows from Lemma 1.1 that the solution of (1.14) with initial value $(y_0, z_0)^T = (0,0)^T$ converges to the equilibrium $Q = (0, c)^T$ for $\varepsilon_1, \varepsilon_2 > 0$. The linearization of (1.14) at Q has eigenvalues $\lambda_1 = -\varepsilon_1 - \varepsilon_2 c$ and $\lambda_2 = 0$ with corresponding eigenvectors $v_1 = (1,0)^T$ and $v_2 = (\varepsilon_1, -\varepsilon_1 - \varepsilon_2 c)^T$. Standard center manifold theory [12] implies that this solution converges to the equilibrium tangent to the center direction v_2.

It turns out that for an asymptotic analysis, a small neighborhood of $(\varepsilon_1, \varepsilon_2)^T = (0,0)^T$ must be divided into four regions corresponding to different singular limits and slow–fast structures in phase space (see Figure 3). Our main result can be summarized as follows.

Theorem 1.5. *There exists $\delta > 0$ such that the following holds in the δ-neighborhood:*

$$D_\delta := \left\{ (\varepsilon_1, \varepsilon_2)^T \in \mathbb{R}^2 \,:\, \varepsilon_1 \geq 0,\, \varepsilon_2 \geq 0,\, \varepsilon_1^2 + \varepsilon_2^2 \leq \delta \right\}$$

of the origin in parameter space.

1. *There exist constants $0 < \beta_3 < \beta_2$ and $\beta_1 > 0$ such that the curves $C_1 = \{(\varepsilon_1, \varepsilon_2)^T \in \mathbb{R}^2 : \varepsilon_1 = \beta_1 \varepsilon_2\}$, $C_2 = \{(\varepsilon_1, \varepsilon_2)^T \in \mathbb{R}^2 : \varepsilon_1 = \beta_2 \varepsilon_2^2\}$, and $C_3 = \{(\varepsilon_1, \varepsilon_2)^T \in \mathbb{R}^2 : \varepsilon_1 = \beta_3 \varepsilon_2^3\}$ divide D_δ into four regions B_{11}, B_{12}, B_2, and B_3 (see Figure 3).*
2. *In each of the regions B_{11}, B_{12}, B_2, and B_3, the problem (1.14) has a different slow–fast structure each depending on a distinguished singular perturbation parameter. These structures become visible in suitable rescalings and blowups.*
3. *For each of these regions B_{11}, B_{12}, B_2, and B_3, we identify a singular orbit γ_0 of a certain type connecting the initial value $O = (0,0)^T$ to the unique equilibrium $Q = (0,c)^T$ of (1.14).*
4. *In each of the regions B_{11}, B_{12}, B_2, and B_3, the orbit corresponding to the initial value approaches the corresponding singular orbit γ_0 in Hausdorff distance as $(\varepsilon_1, \varepsilon_2)^T \to (0,0)^T$ in the respective region, with error estimates depending on the sizes of ε_1, ε_2.*

Remark 1.6 (i). By choosing slightly different constants β_i, the regions B_{11}, B_{12}, B_2, and B_3 can be viewed as overlapping. This implies that the multiscale structure of the solution changes in a smooth way for ε_1, ε_2 close to the curves C_1, C_2, and C_3. (ii) Actually, Theorem 1.5 holds for arbitrary constants $0 < \beta_3 < \beta_2$ and $\beta_1 > 0$ if δ is chosen sufficiently small.

To give a first impression of the different slow–fast structures in these four scaling regions numerically computed solutions of (1.14) are shown in Figure 4. As one moves counterclockwise (increasing ε_2 relative to ε_1), one observes that the plateau value y_{num}^{max} is shrinking and given by $y_{num}^{max} \approx 2.16 \cdot 10^{-2}$, $y_{num}^{max} \approx 6.98 \cdot 10^{-3}$, $y_{num}^{max} \approx 7.05 \cdot 10^{-4}$, $y_{num}^{max} \approx 7.07 \cdot 10^{-5}$, and $y_{num}^{max} \approx 2.26 \cdot 10^{-6}$ in B_{11}, B_{12}, B_2 (lower), B_2 (upper), and B_3, respectively. The structure of these solutions will be explained by relating them to the singular orbits γ_0 of Theorem 1.5. Note that the two solution profiles shown for region B_2 correspond to minor changes in the geometry of the underlying critical manifold (cf. the analysis in Section 3 summarized in Figure 7). In addition, we will show that the numerical values for y_{num}^{max} fit well with corresponding values obtained by our analysis (see Section 6).

Our analysis and proofs are based on suitable blowups of the origin in parameter space which combined with blowups in phase space reveal the underlying slow–fast structures in the regions B_{11}, B_{12}, B_2, and B_3. We are confident that this approach can also be useful in the analysis of systems with more than two singular perturbation parameters.

The rest of the paper is organized as follows: In a first step, it is convenient to blow up the origin in parameter space $(\varepsilon_1, \varepsilon_2)^T = (0,0)^T$ in a suitable way. This is done in Section 2. Loosely speaking, this allows to apply GSPT with the radial parameter as a distinguished singular perturbation parameter. In Section 3, we carry out the rather straightforward GSPT analysis for region B_2. The slow–fast structures corresponding to the regions B_{11}, B_{12}, and B_3 are more complicated and require additional blowups. The analysis of these cases is carried out in in Sections 4 and 5, respectively. We end with a conclusion and outlook.

2 | Structure of Parameter Space

The goal in singularly perturbed systems with a single parameter $\varepsilon \ll 1$ is to prove statements which hold for $\varepsilon \in (0, \hat{\varepsilon}]$ for some $\hat{\varepsilon} > 0$. In system (1.14), we are now dealing with a two-parameter problem in ε_1, $\varepsilon_2 \ll 1$, hence we need to prove results which hold in a small neighborhood of the origin in the parameter space $\mathbb{R}_+^2$.

As a first step, it is instructive to look at the three limiting problems of (1.14):

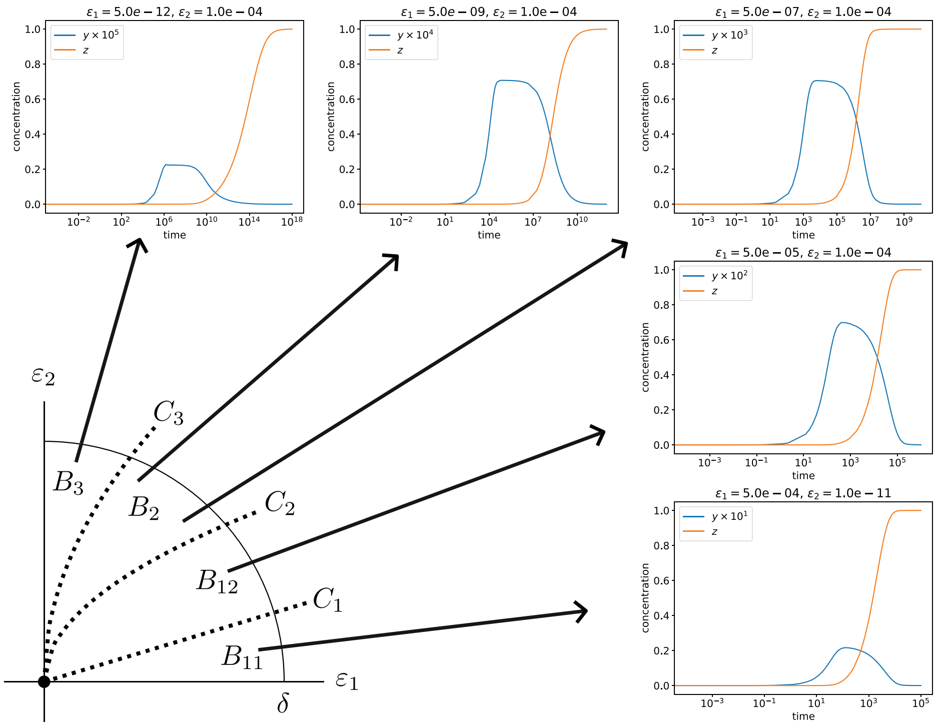

FIGURE 4 | Numerical simulations of (1.14) in different regions of the parameter space for $c = 1$.

1. $\varepsilon_2 = 0,\ \varepsilon_1 > 0$: There exists a unique equilibrium given by $(y,z)^T = (0,c)^T$. The linearization at the equilibrium has one negative and one vanishing eigenvalue, thus center manifold theory can be applied there.
2. $\varepsilon_1 = 0,\ \varepsilon_2 > 0$: The line $y = 0$ consists of equilibria. The line of equilibria $\{(0,z)^T,\ z > 0\}$ is attracting for $\varepsilon_2 > 0$. The origin $(y,z)^T = (0,0)^T$ is more degenerate, that is, the corresponding linearization has a double zero eigenvalue.
3. $\varepsilon_1 = 0 = \varepsilon_2$: The line $y = 0$ consists of degenerate equilibria, that is, the corresponding linearizations have a double-zero eigenvalue.

The three cases above are qualitatively quite different, ranging from a unique equilibrium, which can be analyzed by center manifold reduction, to a very degenerate line of nilpotent equilibria. This indicates that in the double limit we should expect that the relative sizes of ε_1 and ε_2 have a significant influence on the detailed dynamics and asymptotics. It turns out that this is indeed the case and parameter space must be divided into three regions B_1, B_2, and B_3, where

$$\varepsilon_2^2 \ll \varepsilon_1, \quad \varepsilon_1 \approx \varepsilon_2^2, \quad \varepsilon_1 \ll \varepsilon_2^2,$$

respectively. To be precise, we define the curves

$$\begin{aligned} C_2 &:= \left\{(\varepsilon_1,\varepsilon_2)^T \in \mathbb{R}^2 : \varepsilon_1 = \beta_2\varepsilon_2^2\right\}, \\ C_3 &=: \left\{(\varepsilon_1,\varepsilon_2)^T \in \mathbb{R}^2 : \varepsilon_1 = \beta_3\varepsilon_2^2\right\} \end{aligned} \tag{2.1}$$

for $0 < \beta_3 < \beta_2$ and the regions

$$B_1 = \left\{(\varepsilon_1,\varepsilon_2)^T \in \mathbb{R}^2 : \varepsilon_1 > \beta_2\varepsilon_2^2\right\} \tag{2.2}$$

$$B_2 = \left\{(\varepsilon_1,\varepsilon_2)^T \in \mathbb{R}^2 : \beta_3\varepsilon_2^2 \le \varepsilon_1 \le \beta_2\varepsilon_2^2\right\} \tag{2.3}$$

$$B_3 = \left\{(\varepsilon_1,\varepsilon_2)^T \in \mathbb{R}^2 : \varepsilon_1 < \beta_3\varepsilon_2^2\right\}, \tag{2.4}$$

see Figure 5 (left).

To separate the curves C_2 and C_3 in a neighborhood of the origin, we perform a nonhomogeneous blowup transformation. It turns out that this allows for a GSPT analysis in Region B_2, by using the radial parameter as singular perturbation parameter.

The blowup map respecting the scaling properties of the curves C_2 and C_3 is

$$\begin{aligned} &\Phi^1_{par} : [0,\infty) \times \mathbb{S}^1 \to \mathbb{R}^2 \\ &(r,\bar{\varepsilon}_1,\bar{\varepsilon}_2) \mapsto \begin{cases} \varepsilon_1 = r^2\bar{\varepsilon}_1 \\ \varepsilon_2 = r\bar{\varepsilon}_2, \end{cases} \end{aligned} \tag{2.5}$$

where we naturally restrict ourselves to the meaningful parameter space $\bar{\varepsilon}_1, \bar{\varepsilon}_2 \ge 0$. The preimage of the origin under Φ^1_{par} is the quarter circle ($r = 0$), which implies that Φ^1_{par} is not injective for $r = 0$. Away from the origin, the blowup map Φ^1_{par} is a diffeomorphism. In the blown-up parameter space, the quadratic curves C_2 and C_3 correspond to well-separated straight lines $\bar{C}_2$ and $\bar{C}_3$ given by

$$\bar{C}_2 = \left\{(r,\bar{\varepsilon}_1,\bar{\varepsilon}_2)^T \in [0,\infty) \times \mathbb{S}^1 : \bar{\varepsilon}_1 = -1/2\beta_2 + \sqrt{1/4\beta_2^2 + 1}\right\} \tag{2.6}$$

$$\bar{C}_3 = \left\{(r,\bar{\varepsilon}_1,\bar{\varepsilon}_2)^T \in [0,\infty) \times \mathbb{S}^1 : \bar{\varepsilon}_1 = -1/2\beta_3 + \sqrt{1/4\beta_3^2 + 1}\right\} \tag{2.7}$$

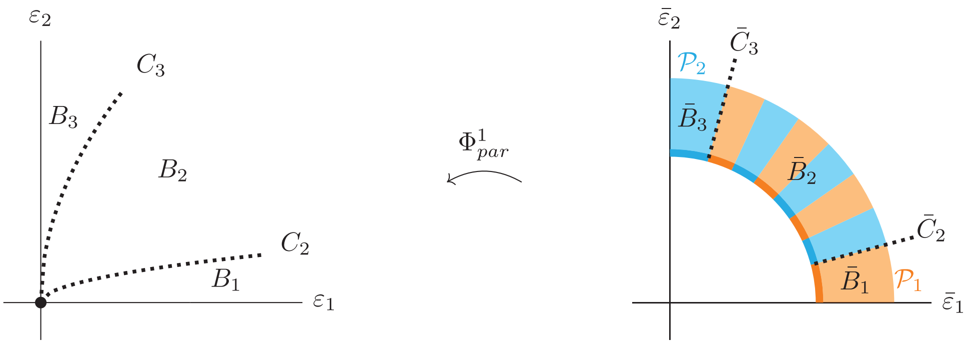

FIGURE 5 | Parameter blowup Φ^1_{par} of the origin and charts $\mathcal{P}_1$ (orange) and $\mathcal{P}_2$ (blue).

with $\beta_3 < \beta_2$ from (2.1), respectively (see Figure 5). The regions B_1, B_2, and B_3 correspond to $\bar{B}_1$, $\bar{B}_2$, and $\bar{B}_3$ in the obvious way. The size of the constants β_2 and β_3 determines the size of the regions $\bar{B}_1$, $\bar{B}_2$, and $\bar{B}_3$. For $\beta_2 \to \infty$, the line $\bar{C}_2$ approaches the $\bar{\varepsilon}_1$-axis, similarly the line $\bar{C}_3$ approaches the $\bar{\varepsilon}_2$-axis as $\beta_3 \to 0$.

Remark 2.1. The choice of the constants β_2 and β_3 determines the size of the neighborhood in which our GSPT analysis is valid. However, for arbitrary constants $0 < \beta_3 < \beta_2$, we can always find such a sufficiently small neighborhood.

It is natural to perform the remaining analysis in directional charts $\mathcal{P}_1$ and $\mathcal{P}_2$ corresponding to the directions $\bar{\varepsilon}_1 = 1$ and $\bar{\varepsilon}_2 = 1$, respectively. In these charts, the blowup transformation has the form

$$\mathcal{P}_1 : \varepsilon_1 = r^2,\ \varepsilon_2 = r\tilde{\varepsilon}_2 \tag{2.8}$$

$$\mathcal{P}_2 : \varepsilon_1 = r^2\tilde{\varepsilon}_1,\ \varepsilon_2 = r, \tag{2.9}$$

respectively. Chart $\mathcal{P}_1$ covers the regions $\bar{B}_1$ and $\bar{B}_2$, while $\mathcal{P}_2$ covers the regions $\bar{B}_2$ and $\bar{B}_3$ (see Figure 5 where the regions covered by charts $\mathcal{P}_1$ and $\mathcal{P}_2$ are shown in orange and blue, respectively). The alternating colors in region $\bar{B}_2$ indicate that this region is covered by both charts.

The regions $\bar{B}_1$ and $\bar{B}_2$ in chart $\mathcal{P}_1$ are given by $0 \le \tilde{\varepsilon}_2 < \sqrt{\frac{1}{\beta_2}}$ and $\sqrt{\frac{1}{\beta_2}} \le \tilde{\varepsilon}_2 \le \sqrt{\frac{1}{\beta_3}}$, respectively. For the analysis in region $\bar{B}_3$, its description in chart $\mathcal{P}_2$, that is, $0 \le \tilde{\varepsilon}_1 < \beta_3$, will be relevant.

We start with the analysis in region $\bar{B}_2$, which is the simplest case and covers the slow–fast structure corresponding to the classical parameters (1.2). The regions $\bar{B}_1$ and $\bar{B}_3$ correspond to more degenerate cases and somewhat more complicated slow–fast structures, which we will treat afterward.

3 | Analysis in Region B_2

The analysis in region $\bar{B}_2$ can be carried out in any of the two charts $\mathcal{P}_i$, $i = 1, 2$, we choose to work in chart $\mathcal{P}_1$. Inserting (2.8) into (1.14), we obtain a slow–fast system in nonstandard form

$$\begin{aligned} y' &= r^2(c - y - z) - y^2 - r\tilde{\varepsilon}_2 yz \\ z' &= y^2, \end{aligned} \tag{3.1}$$

where $r, \tilde{\varepsilon}_2 \in \mathbb{R}_{\ge 0}$. It will be important that in region $\bar{B}_2$ we have $\tilde{\varepsilon}_2 \in \left[\sqrt{\frac{1}{\beta_2}}, \sqrt{\frac{1}{\beta_3}}\right]$. This avoids degeneracies occurring as $\tilde{\varepsilon}_2 \to 0$ or $\tilde{\varepsilon}_2 \to \infty$ which are treated in the analysis of regions $\bar{B}_1$ and $\bar{B}_3$. For better readability, we are dropping the "~" in the following.

In system (3.1), the parameter r is the slow–fast parameter. The layer problem ($r = 0$) has the simple form

$$\begin{aligned} y' &= -y^2 \\ z' &= y^2, \end{aligned} \tag{3.2}$$

which obviously coincides with the limit problem $\varepsilon_1 = \varepsilon_2 = 0$ of (1.14). System (3.2) is explicitly solvable and its orbits are straight lines with slope -1, that is,

$$z = -y + s, \quad s \in \mathbb{R}.$$

As mentioned before, $y = 0$ is a line of nilpotent equilibria which attracts all orbits with $y(0) > 0$ in forward time and attracts all orbits with $y(0) < 0$ in backward time. As a consequence of this degeneracy, solutions are very sensitive to perturbations around $y = 0$. Note that the initial value $O = (0, 0)^T$ and also the unique equilibrium $Q = (0, c)^T$ of (3.1) lie on the line of equilibria $y = 0$ represented by a teal and black dot in Figure 6, respectively.

In terms of slow–fast systems, the critical manifold $\mathcal{S}$ is given by

$$\mathcal{S} = \left\{(y, z)^T \in \mathbb{R}^2 : y = 0\right\},$$

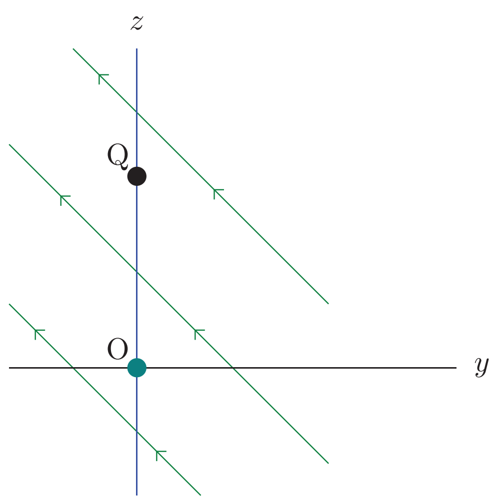

FIGURE 6 | Phase portrait of the layer problem (3.2).

which is not normally hyperbolic (which is indicated by green simple arrows in Figure 6). Due to the lack of normal hyperbolicity, Fenichel theory is not applicable. We resolve this degeneracy by rescaling the variable y with

$$y = r\tilde{y}. \tag{3.3}$$

Inserting (3.3) into (3.1) gives

$$\begin{aligned} \tilde{y}' &= r(c - r\tilde{y} - z - \tilde{y}^2 - \varepsilon_2 \tilde{y} z) \\ z' &= r^2 \tilde{y}^2. \end{aligned} \tag{3.4}$$

For $r = 0$, this vector field vanishes identically, thus we desingularize the system by dividing out a factor r, which can be viewed as transforming to a slower time scale. Clearly, this does not change the orbits of the system. This leads to

$$\begin{aligned} \tilde{y}' &= c - r\tilde{y} - z - \tilde{y}^2 - \varepsilon_2 \tilde{y} z \\ z' &= r\tilde{y}^2. \end{aligned} \tag{3.5}$$

System (3.5) is of standard slow–fast form with respect to the singular perturbation parameter r. To simplify the notation in the following computations, we drop the "~" and obtain

$$\begin{aligned} y' &= c - ry - z - y^2 - \varepsilon_2 yz \\ z' &= ry^2, \end{aligned} \tag{3.6}$$

which will be the starting point for the analysis throughout the rest of the analysis in Sections 3 and 4.

For $r = 0$, we obtain the layer problem

$$\begin{aligned} y' &= c - z - y^2 - \varepsilon_2 yz \\ z' &= 0. \end{aligned} \tag{3.7}$$

The critical manifold is $\mathcal{S} = \{(x, y)^T \in \mathbb{R}^2 : c - z - y^2 - \varepsilon_2 yz = 0\}$. In the following, we focus on the part of $\mathcal{S}$ in the half plane $y \geq 0$, denoted by $\mathcal{S}^a$, which is normally attracting for $\varepsilon_2 \in \left[\sqrt{\frac{1}{\beta_2}}, \sqrt{\frac{1}{\beta_3}}\right]$ and can be described as a graph

$$z = \frac{c - y^2}{1 + \varepsilon_2 y}. \tag{3.8}$$

The hyperbolicity of $\mathcal{S}^a$ follows since the eigenvalue of the corresponding linearization of (3.7) is $\lambda_1 = -2y - \varepsilon_2 z < 0$. Note that $\mathcal{S}^a$ intersects the positive y-axis at $y = y^{max} := \sqrt{c}$ (see Figure 7).

The parameter ε_2 changes the geometry of the critical manifold $\mathcal{S}$, compare Figure 7 where $\mathcal{S}$ is shown in blue. These changes are due to the occurrence of a transcritical bifurcation of $\mathcal{S}$ at $(y, z)^T = (-\sqrt{c}, 2c)^T$ for $\frac{1}{\varepsilon_2^2} = c$. We do not study this in detail since it occurs in the nonphysical part of phase space. For $\varepsilon_2 \in \left[\sqrt{\frac{1}{\beta_2}}, \sqrt{\frac{1}{\beta_3}}\right]$, these changes do not affect normal hyperbolicity of $\mathcal{S}^a$. For $\varepsilon_2 \to 0$, however, the fold point of $\mathcal{S}$ approaches the equilibrium Q. In the limit $\varepsilon_2 = 0$, the critical manifold is given by

$$z = c - y^2,$$

that is, the fold point of the critical manifold coincides with the equilibrium $Q = (0, c)^T$ (see Figure 8a). For $\varepsilon_2 \to \infty$, the critical manifold $\mathcal{S}$ approaches the y- and z-axis (see Figure 8b). In these two limits, normal hyperbolicity of $\mathcal{S}^a$ is lost at Q and O, respectively.

Since we stay away from these degenerate limits in region $\bar{B}_2$, the following construction of singular orbits and proof of their persistence based on Fenichel theory works for all ε_2 in region $\bar{B}_2$. In particular, the compact part of $\mathcal{S}^a$ connecting y^{max} and the equilibrium $Q = (0, c)^T$

$$\gamma_0^s = \left\{(y, z)^T \in \mathcal{S}^a : y \in [0, y^{max}]\right\} \tag{3.9}$$

is normally attracting (which is indicated by green double arrows in Figure 7). The first part of the singular orbit, which connects the initial value $O = (0, 0)^T$ along the fast fiber (green) with the point $(y^{max}, 0)^T \in \mathcal{S}^a$ is given by

$$\gamma_0^f = \left\{(y, 0)^T \in \mathbb{R}^2 : y \in [0, y^{max}]\right\}. \tag{3.10}$$

It remains to check the reduced flow on $\mathcal{S}^a$. We change to the slow time scale $t = r\tau$ and obtain the reduced flow on $\mathcal{S}^a$

$$\dot{z} = y^2 \geq 0, \tag{3.11}$$

where " $\cdot$ " denotes differentiation with respect to t. Thus, the solution of the reduced problem starting at $(y^{max}, 0)^T$ converges

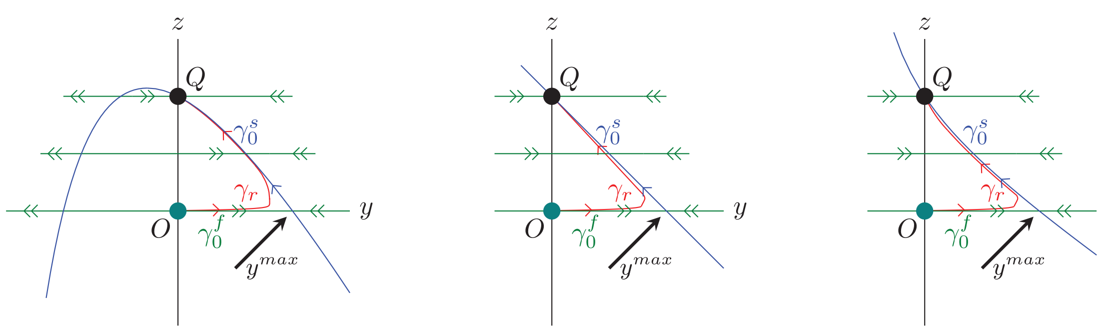

(a) $\frac{1}{\varepsilon_2^2} > c$. (b) $\frac{1}{\varepsilon_2^2} = c$. (c) $\frac{1}{\varepsilon_2^2} < c$.

FIGURE 7 | Singular orbit structure (green and blue) of (3.6) and genuine orbit (red) connecting O and Q for $0 < r \ll 1$.

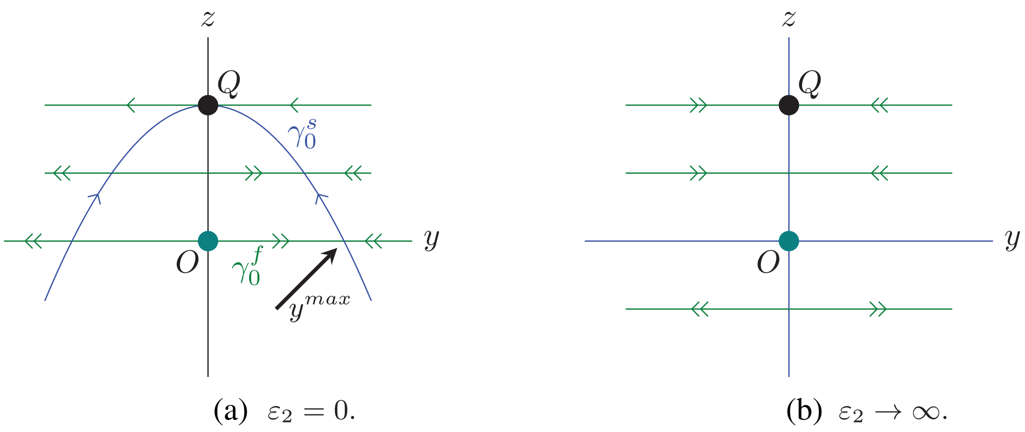

FIGURE 8 | Limits of the singular dynamics of (3.6).

center-like, that is, with an algebraic rate, to the equilibrium $Q = (0, c)^T$. We obtain the following lemma.

Lemma 3.1. *There exists a singular orbit $\gamma_0 := \gamma_0^f \cup \gamma_0^s$ of (3.7) connecting the initial value O and the equilibrium Q.*

Due to the following theorem, the singular orbit perturbs to a genuine orbit for r small.

Theorem 3.2. *There exists $r_0 > 0$ such that for all $\varepsilon_2 \in \left[\sqrt{\frac{1}{\beta_2}}, \sqrt{\frac{1}{\beta_3}}\right]$ and $r \in (0, r_0]$ there exists a smooth orbit γ_r of system (3.6), connecting the initial value $O = (0,0)^T$ with the equilibrium $Q = (0, c)^T$. The perturbed orbit γ_r is $\mathcal{O}(r)$-close to γ_0 in Hausdorff distance.*

Proof. The normally hyperbolic attracting critical manifold S^a perturbs to an attracting slow manifold S_r^a by Fenichel theory for $0 < r \ll 1$, which contains the equilibrium Q. Since there are no further equilibria for $r > 0$ the slow flow on S_r^a converges to Q for $y \geq 0$ (as a center flow). Viewed as an equilibrium of system (3.6), Q has a two-dimensional center-stable manifold W^{cs} which intersects S_r^a transversally. By Fenichel theory, the solution with initial value O, that is, the orbit γ_r, is attracted exponentially onto S_r^a and hence converges to Q in the center direction. By construction, γ_r is $\mathcal{O}(r)$ close to γ_0. ☐

We conclude that for all $(\varepsilon_1, \varepsilon_2)^T \in B_2$ with $||(\varepsilon_1, \varepsilon_2)^T|| < r_0$ there exists a smooth orbit γ_{ε_1} of system (1.14), which is $\mathcal{O}(\sqrt{\varepsilon_1})$-close to γ_0 in Hausdorff distance, connecting the initial value O with the equilibrium Q.

A possibility to compare our asymptotic results with the numerics is the maximal value of the y-component y^{max}, which we will focus on in the following. Due to the extra rescaling (3.3), we even achieve an error estimate of $\mathcal{O}(\varepsilon_1)$ in y-direction. Indeed, by undoing the rescalings (2.8) and (3.3), we obtain

$$y = r\tilde{y} = \sqrt{\varepsilon_1}\tilde{y}. \tag{3.12}$$

Along the singular orbit γ_0, we have

$$\max\left\{\tilde{y} : (\tilde{y}, z)^T \in \gamma_0\right\} = \tilde{y}^{max} = \sqrt{c},$$

such that

$$y^{max} = \sqrt{\varepsilon_1}(\sqrt{c} + \mathcal{O}(\sqrt{\varepsilon_1})) = \sqrt{\varepsilon_1 c} + \mathcal{O}(\varepsilon_1).$$

Inserting the parameter values (1.2) of the original problem gives

$$y^{max} = 3.651 \cdot 10^{-5} + \mathcal{O}(10^{-9}), \tag{3.13}$$

which fits well with the value obtained by numerical simulations, for example, compare with Figure 2. In particular, this confirms the numerical results in [14].

Remark 3.3. From the blowup point of view, the rescaling (3.3) can be viewed as the scaling chart of a cylindrical blowup of the degenerate line $(0, z, 0)$, $z \in \mathbb{R}$ in extended (y, z, r) phase space. Since this scaling chart covers the relevant dynamics, there is no need to introduce this blowup explicitly.

It remains to do the analysis of the degenerate cases corresponding to $\tilde{\varepsilon}_2 \to 0$ and $\tilde{\varepsilon}_2 \to \infty$ in regions $\bar{B}_1$ and $\bar{B}_3$, respectively. We start with the region $\bar{B}_1$, since this allows us to continue in the current chart $\mathcal{P}_1$.

4 | Analysis in Region B_1

The starting point of the following analysis in chart $\mathcal{P}_1$ are Equations (3.6), which we restate here for convenience

$$\begin{aligned} y' &= c - ry - z - y^2 - \tilde{\varepsilon}_2 yz \\ z' &= ry^2. \end{aligned} \tag{4.1}$$

As described before, for $\tilde{\varepsilon}_2 \to 0$ the fold point of $\mathcal{S}$ is at $Q = (0, c)^T$ (see Figure 8a). To treat this loss of normal hyperbolicity, we perform a blowup of the fold point $(0, c, 0)^T$ in extended $(y, z, \tilde{\varepsilon}_2)^T$ space. To handle the terms $-ry$ and $-\tilde{\varepsilon}_2 yz$ in (4.1), an additional homogeneous parameter blowup of the origin $(r, \tilde{\varepsilon}_2)^T = (0, 0)^T$ in chart $\mathcal{P}_1$ is introduced. Otherwise, we would not be able to desingularize the dynamics in the blowup of the fold point. In the original parameters, the second parameter blowup amounts to dividing the region B_1 into two parts B_{11} and B_{12} by a curve

$$C_1 := \left\{(\varepsilon_1, \varepsilon_2)^T \in \mathbb{R}^2 : \varepsilon_1 = \beta_1 \varepsilon_2\right\} \tag{4.2}$$

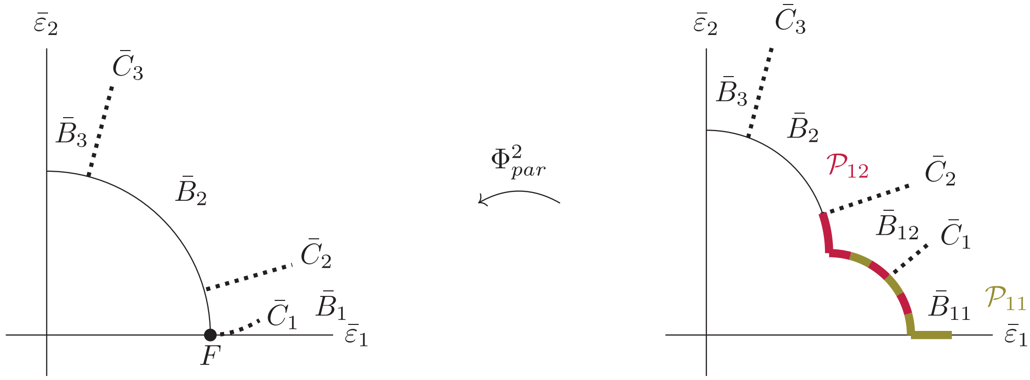

FIGURE 9 | Schematic picture of the parameter blowup Φ^2_{par} of the point F (corresponding to the origin in chart $\mathcal{P}_1$) shown in blown-up $(\mathbb{R} \times \mathbb{S}^1)$-space.

with some $\beta_1 > 0$. The parts B_{11} and B_{12} correspond to scaling regimes $0 \leq \varepsilon_2 \lesssim \varepsilon_1$ and $\varepsilon_2^2 \ll \varepsilon_1 \lesssim \varepsilon_2$, respectively. The second parameter blowup map is given by

$$\Phi^2_{par} : [0, \infty) \times \mathbb{S}^1 \to \mathbb{R}^2$$

$$(s, \bar{r}, \bar{\tilde{\varepsilon}}_2) \mapsto \begin{cases} r = s\bar{r} \\ \tilde{\varepsilon}_2 = s\bar{\tilde{\varepsilon}}_2. \end{cases} \tag{4.3}$$

In the blown-up space, the curve C_1 corresponds to the line

$$\bar{\varepsilon}_2 = \sqrt{\frac{1}{1 + \beta_1^2}}.$$

Again, it is convenient to perform the analysis in two charts corresponding to the directions $\bar{r} = 1$ and $\bar{\varepsilon}_2 = 1$, respectively. In these charts, the blowup transformation Φ^2_{par} is given by

$$\mathcal{P}_{11} : r = s,\ \tilde{\varepsilon}_2 = s\varepsilon_{21}, \tag{4.4}$$

$$\mathcal{P}_{12} : r = sr_1, \tilde{\varepsilon}_2 = s \tag{4.5}$$

such that in chart $\mathcal{P}_{11}$ the regions B_{11} and B_{12} in the blown-up space are given by $\varepsilon_{21} < \beta_1$ and $\varepsilon_{21} \geq \beta_1$, respectively. A schematic representation of the second blowup in parameter space is shown in Figure 9. As can be seen in Figure 9, chart $\mathcal{P}_{11}$ will be used for analyzing the limit $\tilde{\varepsilon}_2 \to 0$ in region $\bar{B}_{11}$, whereas chart $\mathcal{P}_{12}$ covers region $\bar{B}_{12}$. We begin with the analysis in chart $\mathcal{P}_{11}$.

4.1 | Analysis in Region B_{11}

Inserting the parameter blowup transformation (4.4) into (4.1), we obtain

$$\begin{aligned} y' &= c - sy - z - y^2 - s\varepsilon_{21}yz \\ z' &= sy^2. \end{aligned} \tag{4.6}$$

In the following analysis, it will be important that $\varepsilon_{21} \in [0, \beta_1]$. System (4.6) is of classical slow–fast type with parameter s. The critical manifold is given by

$$\mathcal{S} = \left\{(y, z)^T \in \mathbb{R}^2 : z = c - y^2\right\}$$

with a fold point at the equilibrium $Q = (0, c)^T$ (see again Figure 8). The candidate singular orbit starting from the initial value $O = (0, 0)^T$ is again $\gamma_0 = \gamma_0^f \cup \gamma_0^s$, but it approaches Q along the slow manifold $\mathcal{S}$, which loses normal hyperbolicity at the fold point. Therefore, we cannot use Fenichel theory directly to prove convergence to the genuine equilibrium along γ_0. We resolve this degeneracy by artificially adding $s' = 0$ to (4.6) and applying a spherical blowup of the nilpotent point $(y, z, s)^T = (0, c, 0)^T$ of this extended system, see [24] for a detailed explanation of the blowup method in the context of planar fold points.

The suitable blowup transformation is given by

$$\Phi : [0, \infty) \times \mathbb{S}^2 \to \mathbb{R}^3$$

$$(\sigma, \bar{y}, \bar{z}, \bar{s}) \mapsto \begin{cases} y = \sigma\bar{y} \\ z = c + \sigma^2\bar{z} \\ s = \sigma\bar{s}. \end{cases} \tag{4.7}$$

The nilpotent point $(0, c, 0)^T$ is blown up to the sphere $\{0\} \times \mathbb{S}^2$, which is the preimage of $(0, c, 0)^T$ under the map Φ (see Figure 10).

Remark 4.1. Note that in the transformation (4.7) the weights of the radial variable σ deviate from the weights in the analysis of the generic fold point. This is a consequence of the fold point coinciding with an equilibrium in our case.

Much of the following analysis proceeds along the lines of [24], the dynamics on the sphere $\sigma = 0$ is, however, different from the standard fold point, so we give the necessary details. Again, it will be convenient to work in directional charts which correspond to directions $\bar{y} = 1$, $\bar{s} = 1$, and $\bar{z} = -1$. The blowup transformation in these charts is given by

$$\mathcal{K}^1_{11} : y = \sigma_1, \quad z = c + \sigma_1^2 z_1, \quad s = \sigma_1 s_1 \tag{4.8}$$

$$\mathcal{K}^2_{11} : y = \sigma_2 y_2, \quad z = c + \sigma_2^2 z_2, \quad s = \sigma_2 \tag{4.9}$$

$$\mathcal{K}^3_{11} : y = \sigma_3 y_3, \quad z = c - \sigma_3^2, \quad s = \sigma_3 s_3, \tag{4.10}$$

respectively. Note that subscripts refer to the parameter blowup chart, whereas a superscript denotes the corresponding chart in phase space. Chart $\mathcal{K}^1_{11}$ covers the right $(\bar{y} > 0)$ side of the sphere,

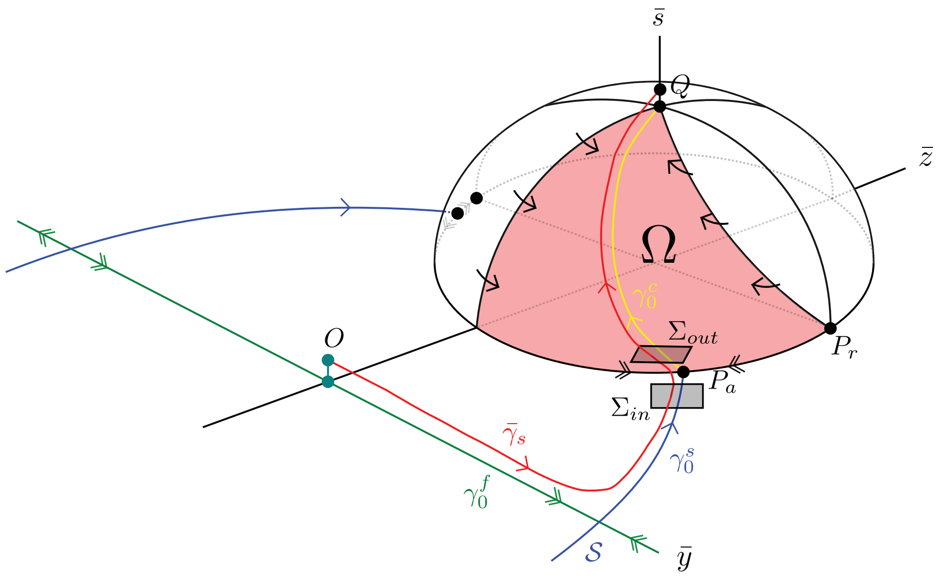

FIGURE 10 | Dynamics of the blown-up extended system (4.6).

chart $\mathcal{K}_{11}^2$ covers the top ($\bar{s} > 0$) of the sphere, and chart $\mathcal{K}_{11}^3$ covers the front ($\bar{z} < 0$) side of the sphere (see Figure 10).

Remark 4.2. For blowups in phase space, we will often follow the useful convention, that an object A is denoted as A_i in a chart $\mathcal{K}^i$, $i = 1, 2, 3$ in which the blowup is studied. As an example, consider the equilibrium Q which will be studied in chart $\mathcal{K}_{11}^2$ and is denoted as Q_2 there.

The following subset of the sphere is central for our analysis.

Definition 4.3. Let Ω be the compact subset of the sphere ($\sigma = 0$) enclosed by the equator ($\bar{s} = 0$), the meridian ($\bar{y} = 0$), and the curve which is represented by $s_1 = -z_1$ in chart $\mathcal{K}_{11}^1$ and $z_2 = -y_2$ in chart $\mathcal{K}_{11}^2$ (see Figure 10 where Ω is shown in red).

We have the following result.

Lemma 4.4. *The flow of the blown-up vector field on the sphere has the properties:*

i. *The set Ω is forward invariant.*

ii. *There exists a heteroclinic orbit γ_0^c connecting the endpoint P_a of $\mathcal{S}$ with the equilibrium Q.*

Proof. We start the analysis in chart $\mathcal{K}_{11}^1$, which is one of the entrance charts since it contains the endpoint P_a of the attracting branch of the critical manifold $\mathcal{S}$, denoted by $\mathcal{S}^a$, with reduced flow toward the sphere. Inserting (4.8) into (4.6) and after desingularizing, that is, dividing out a factor of σ_1, we obtain

$$\begin{aligned} z_1' &= s_1 + 2z_1\left(s_1 + z_1 + 1 + \sigma_1^2\varepsilon_{21}s_1z_1 + s_1\varepsilon_{21}c\right) \\ s_1' &= s_1\left(s_1 + z_1 + 1 + \sigma_1^2\varepsilon_{21}s_1z_1 + s_1\varepsilon_{21}c\right) \\ \sigma_1' &= -\sigma_1\left(s_1 + z_1 + 1 + \sigma_1^2\varepsilon_{21}s_1z_1 + s_1\varepsilon_{21}c\right). \end{aligned} \tag{4.11}$$

The planes $\sigma_1 = 0$ and $s_1 = 0$ are invariant. They intersect in a line, which corresponds to a part of the equator of the sphere, on which the dynamics is governed by $z_1' = 2z_1(z_1 + 1)$. There are two equilibria $P_a = (-1, 0, 0)^T$ and $P_r = (0, 0, 0)^T$ which are attracting and repelling on this line with eigenvalues -2 and 2, respectively.

On the plane $s_1 = 0$, the dynamics is given by

$$\begin{aligned} z_1' &= 2z_1(z_1 + 1) \\ \sigma_1' &= -\sigma_1(z_1 + 1). \end{aligned} \tag{4.12}$$

The normally attracting line of equilibria

$$z_1 = -1$$

corresponds to the attracting branch of the critical manifold $\mathcal{S}^a$ (see Figure 10). We now investigate the dynamics on the plane $\sigma_1 = 0$ (on the sphere) near the point P_a governed by

$$\begin{aligned} z_1' &= s_1 + 2z_1(s_1 + z_1 + 1 + s_1\varepsilon_{21}c) \\ s_1' &= s_1(s_1 + z_1 + 1 + s_1\varepsilon_{21}c). \end{aligned} \tag{4.13}$$

We recover the equilibria P_a and P_r. The eigenvalues of the linearization at P_a and P_r are -2, 0 and 2, 1, respectively. We conclude that P_r is a source on the sphere. Standard center manifold theory [12] implies the existence of an attracting one-dimensional center manifold N_a at P_a, which is given as a graph $z_1 = h_1(s_1)$ with expansion

$$h_1(s_1) = -1 - \left(\frac{1}{2} + \varepsilon_{21}c\right)s_1 + \mathcal{O}\left(s_1^2\right). \tag{4.14}$$

The corresponding flow on N_a is governed by

$$s_1' = s_1^2/2 + \mathcal{O}\left(s_1^3\right),$$

hence z_1 increases along N_a. This implies that the branch of N_a in $s_1 > 0$ is unique. For proving assertion (ii), it remains to show that the continuation of this branch of N_a by the flow connects P_a with the equilibrium Q (which is only visible in the scaling chart

$\mathcal{K}_{11}^2$). This is done in the following by first proving assertion (i) and using a phase plane argument.

The part of $\partial\Omega$ that is visible in chart $\mathcal{K}_{11}^1$ is given by the invariant half line $s_1 = 0$ and the line $s_1 = -z_1$, respectively, both with $z_1 \leq 0$. On these half lines, the flow cannot exit Ω. For the line $s_1 = -z_1$, this follows from

$$(s_1 + z_1)'|_{s_1=-z_1} = -s_1^2 \varepsilon_{21} c \leq 0 \tag{4.15}$$

for all $\varepsilon_{21} \geq 0$ (see [1, p. 219]).

Now we switch to the chart $\mathcal{K}_{11}^3$ in which the governing equations are

$$\begin{aligned} y_3' &= -y_3 s_3 + 1 - y_3^2 + \sigma_3^2 \varepsilon_{21} y_3 s_3 - s_3 \varepsilon_{21} y_3 c + \frac{1}{2} y_3^3 s_3 \\ s_3' &= \frac{1}{2} y_3^2 s_3^2 \\ \sigma_3' &= -\frac{1}{2} \sigma_3 y_3^2 s_3. \end{aligned} \tag{4.16}$$

On the invariant plane $s_3 = 0$, we recover the two normally hyperbolic parts of the critical manifold as lines of equilibria

$$y_3 = \pm 1,$$

where the attracting line $y_3 = 1$ terminates in P_a. Clearly, this chart also covers the center manifold N_a originating at P_a.

The part of $\partial\Omega$ on the sphere $\sigma = 0$ that is visible in chart $\mathcal{K}_{11}^3$ is given by the invariant half line $s_3 = 0$, $y_3 \geq 0$ and the half line $y_3 = 0$, $s_3 \geq 0$. The flow on the sphere cannot leave Ω at these half lines. For the line $y_3 = 0$, $s_3 \geq 0$ this follows from $y_3' = 1$.

To cover the part of Ω close to Q, we change to the scaling chart $\mathcal{K}_{11}^2$ where we can trace γ_0^c once it has entered Ω. The dynamics in the scaling chart $\mathcal{K}_{11}^2$ is governed by

$$\begin{aligned} y_2' &= -y_2 - z_2 - y_2^2 - y_2 \varepsilon_{21} c - \sigma_2^2 z_2 y_2 \varepsilon_{21} \\ z_2' &= y_2^2 \\ \sigma_2' &= 0. \end{aligned} \tag{4.17}$$

On the invariant sphere $\sigma = 0$, this simplifies to

$$\begin{aligned} y_2' &= -y_2 - z_2 - y_2^2 - y_2 \varepsilon_{21} c \\ z_2' &= y_2^2. \end{aligned} \tag{4.18}$$

The boundary of Ω in $\bar{s} > 0$ is given by parts of the lines $y_2 = 0$, $z_2 \leq 0$,z and $z_2 = -y_2$, $y_2 \geq 0$. The flow of (4.18) cannot leave Ω at these parts of the boundary since

$$y_2' = -z_2$$

on the line $y_2 = 0$ and

$$(y_2 + z_2)' = -y_2 \varepsilon_{21} c \leq 0$$

on the line $z_2 = -y_2$. We conclude that Ω is indeed a compact forward invariant trapping region on the sphere. This concludes the proof of assertion (i).

In chart $\mathcal{K}_{11}^2$, the equilibrium Q corresponds to the point $Q_2 = (0,0)^T$. The linearization of (4.18) at Q_2 has eigenvalues $\lambda_s = -1 - \varepsilon_{21} c$ and $\lambda_c = 0$ with corresponding eigenvectors $v_s = (1,0)^T$ and $v_c = (1, -1 - \varepsilon_{21} c)^T$. Standard center manifold theory implies the existence of an attracting (nonunique) center manifold W^c, which lies in the interior of Ω for $\varepsilon_{21} > 0$ and coincides with the line $z_2 = -y_2$ in the limiting case $\varepsilon_{21} = 0$. The flow on the center manifold W^c in Ω is directed toward the equilibrium Q_2. There are no equilibria in the interior of Ω such that we can exclude periodic orbits. The only equilibrium in the forward invariant compact set Ω which is not repelling is the equilibrium $Q_2 \subset \partial\Omega$. On the sphere $\sigma = 0$, the Poincaré–Bendixson theorem applies, therefore all orbits within Ω must converge to the equilibrium Q_2 along the center manifold W^c. Therefore, the continuation of the N_a in $s_1 > 0$ converges to Q_2. We denote the corresponding heteroclinic orbit by γ_0^c, which is shown in yellow in Figure 10. This proves assertion (ii). □

By collecting the results of this subsection, we obtain

Lemma 4.5. *There exists a singular orbit γ_0 of the blown-up extended system (4.6) connecting the initial value O, via P_a, with the equilibrium Q.*

Proof. Starting from the initial value O, we follow γ_0^f and γ_0^s as before. In the blown-up problem, γ_0^s terminates in the point P_a. From there, we follow γ_0^c which connects P_a and Q. We define the singular orbit as $\gamma_0 := \gamma_0^f \cup \gamma_0^s \cup \gamma_0^c$ (see Figure 10). □

Now we prove that the singular orbit γ_0 perturbs to a smooth orbit γ_s connecting the initial condition O and the equilibrium Q for $0 < s \ll 1$.

Theorem 4.6. *There exists a constant $\tilde{s} > 0$ such that for all $\varepsilon_{21} \in [0, \beta_1]$ and $s \in (0, \tilde{s}]$, there exists a smooth orbit γ_s of (4.6) connecting the initial value O and the equilibrium Q. The corresponding orbit $\bar{\gamma}_s$ in blown-up space is $\mathcal{O}(s)$-close to γ_0 in Hausdorff distance.*

Proof. The proof is carried out in the blowup of system (4.6) extended by $s' = 0$. In a first step, we show that the continuation of the slow manifold by the flow, which exist by Fenichel theory away from the fold, converges to the equilibrium Q. For this purpose, we define two sections in the entrance chart $\mathcal{K}_{11}^1$ close to P_a as

$$\Sigma_{in} := \left\{ (z_1, s_1, \sigma_1)^T \in \mathbb{R}^3 \, : \, \sigma_1 = a, \, |z_1 + 1| < b, \, s_1 < a \right\} \tag{4.19}$$

and

$$\Sigma_{out} := \left\{ (z_1, s_1, \sigma_1)^T \in \mathbb{R}^3 \, : \, \sigma_1 < a, \, |z_1 + 1| < b, \, s_1 = a \right\} \tag{4.20}$$

with $a, b > 0$ small enough (see Figure 10). Away from the sphere $\sigma = 0$, the attracting branch $\mathcal{S}^a$ of the critical manifold perturbs to an attracting slow manifold $\mathcal{S}_s^a$ for $s \ll 1$ by Fenichel theory. In extended phase space, this one-parameter family of slow manifolds can be viewed as a two-dimensional invariant attracting slow manifold $\mathcal{M}$. The manifold $\mathcal{M}$ is defined at least up to the section Σ_{in}. We extend the manifold $\mathcal{M}$ by the forward flow of the blown-up vector field past Σ_{in}, the corresponding larger manifold is still denoted as $\mathcal{M}$. The results in [24] on the standard singularly perturbed fold point imply that $\mathcal{M}$ is attached to the orbit γ_0^c. Therefore, we can track $\mathcal{M}$ across the sphere for s small. In the blown-up phase space, the equilibrium Q corresponds to a line of equilibria $(0,0,\sigma_2)^T$, $\sigma_2 \in [0,\tilde{s}]$. The linearization along this line of equilibria has one negative and a double zero eigenvalue. Standard invariant manifold theory implies the existence of a three-dimensional center-stable manifold W^{cs} of this line of equilibria. Since the orbit γ_0^c on the sphere intersects W^{cs} transversely, the manifold $\mathcal{M}$ also intersects W^{cs} since it is a small smooth perturbation of γ_0^c for $s \ll 1$. This implies that all orbits in $\mathcal{M}$ converge to Q.

Viewed in chart $\mathcal{K}_{11}^3$ of the extended blown-up phase space, the line of initial conditions $\{(0,0,s)^T,\ s \in [0,\tilde{s}]\}$ corresponds to the line $(0,\sqrt{c},\frac{s}{\sqrt{c}})^T$, $s \in [0,\tilde{s}]$. All orbits starting on this line are exponentially attracted onto the manifold $\mathcal{M}$ by Fenichel theory until they reach Σ_{in}. During the passage from Σ_{in} to Σ_{out}, an additional exponential contraction toward $\mathcal{M}$ occurs due to [24, Proposition 2.8]. Beyond the section Σ_{out}, the evolution of these orbits is governed by system (4.17) with $\sigma_2 \in [0,\tilde{s}]$. Since σ_2 acts as a regular perturbation parameter, these orbits intersect W^{cs} for $\tilde{s}$ sufficiently small. This implies the existence of a smooth perturbed orbit $\bar{\gamma}_s$ connecting the lines of equilibria corresponding to O and Q, respectively. The assertions of the theorem follow by applying the blowup transformation (4.7), that is, $\gamma_s = \Phi(\bar{\gamma}_s)$. □

In order to complete the argument in region $\bar{B}_1$, we use chart $\mathcal{P}_{12}$ which covers the region $\bar{B}_{12}$.

4.2 | Analysis in Region B_{12}

We insert the transformation (4.5) into (4.1) and obtain

$$
\begin{aligned}
y' &= c - sr_1 y - z - y^2 - syz \\
z' &= sr_1 y^2,
\end{aligned}
\tag{4.21}
$$

where s and r_1 are both small. The goal is to construct the orbit connecting O to the equilibrium Q for $(s,r_1)^T$, $r_1 > 0$, $s > 0$ in a small neighborhood of the origin. For $s = 0$, we again obtain the critical manifold

$$z = c - y^2$$

with the equilibrium $Q = (0,c)^T$ at the fold point.

Again, we use the blowup transformation (4.7) to resolve the degeneracy of the fold point and we obtain the following result.

Lemma 4.7. *In the blown-up space of system (4.21) extended by the equation $s' = 0$, there exists for $r_1 = 0$ a two-dimensional attracting critical manifold S^a (blue in Figure 11), which contains the line of equilibria corresponding to the genuine equilibrium Q. The critical manifold S^a perturbs regularly to a slow manifold $S^a_{r_1}$ for r_1 small enough. All orbits of the reduced flow on S^a approach the line of equilibria in the center direction, that is, with an algebraic rate, for all $0 < s \le 1/\sqrt{\beta_2}$.*

Proof. We carry out the analysis in two directional charts

$$\mathcal{K}_{12}^2 : y = \sigma_2 y_2, \quad z = c + \sigma_2^2 z_2, \quad s = \sigma_2 \tag{4.22}$$

$$\mathcal{K}_{12}^3 : y = \sigma_3 y_3, \quad z = c - \sigma_3^2, \quad s = \sigma_3 s_3 \tag{4.23}$$

covering the top $\bar{s} > 0$ and the front $\bar{z} < c$ part of the sphere, respectively (see Figure 11). The parts of S^a investigated in chart $\mathcal{K}_{12}^2$ and $\mathcal{K}_{12}^3$ are denoted by S^a_2 and S^a_3, respectively.

As before, we start the analysis in the entrance chart $\mathcal{K}_{12}^3$. By inserting (4.23) into (4.21) and desingularizing by dividing out a factor σ_3, we obtain

$$
\begin{aligned}
y_3' &= 1 - y_3^2 - y_3 s_3 c + \sigma_3^2 s_3 y_3 + r_1\left(s_3 y_3 + \frac{1}{2}s_3 y_3^3\right) \\
s_3' &= \frac{1}{2} r_1 s_3^2 y_3^2 \\
\sigma_3' &= -\frac{1}{2} r_1 \sigma_3 s_3 y_3^2.
\end{aligned}
\tag{4.24}
$$

Note that system (4.24) is of standard slow–fast type with singular perturbation parameter r_1 and corresponding layer problem

$$
\begin{aligned}
y_3' &= 1 - y_3^2 - y_3 s_3 c + \sigma_3^2 s_3 y_3 \\
s_3' &= 0 \\
\sigma_3' &= 0.
\end{aligned}
\tag{4.25}
$$

For $r_1 = 0$, we find the two-dimensional critical manifold

$$\mathcal{S}_3 = \left\{(y_3,s_3,\sigma_3)^T \in \mathbb{R}^3 : 1 - y_3^2 - y_3 s_3 c + \sigma_3^2 s_3 y_3 = 0\right\}, \tag{4.26}$$

which for $s_3 = 0$ reduces to the two lines of equilibria $y_3 = \pm 1$.

Remark 4.8. Note that here the variable σ_3 changes the geometry of the critical manifold $\mathcal{S}_3$ and r_1 is the singular perturbation parameter. In terms of the original system (1.14), this means that—loosely speaking—ε_2 changes the geometry and ε_1 is the singular perturbation parameter. We will see that these roles will be switched when we study the dynamics in region B_3.

The eigenvalue of the linearization of the layer problem (4.25) is $\lambda = -2y_3 - s_3(c - \sigma_3^2)$. At the line $s_3 = 0$, $y_3 = 1$, we obtain

$$\lambda = -2 < 0$$

and we conclude that the line $s_3 = 0, y_3 = 1$ is part of the attracting branch S^a_3 of the critical manifold, which extends regularly into $s_3 > 0$, since s_3 acts as a regular perturbation parameter in (4.26).

The reduced flow on S^a_3 is given by

$$
\begin{aligned}
\dot{s}_3 &= \frac{1}{2} s_3^2 y_3^2 \\
\dot{\sigma}_3 &= -\frac{1}{2}\sigma_3 s_3 y_3^2.
\end{aligned}
\tag{4.27}
$$

For $s_3 = 0$, the reduced flow along S^a_3 is stationary, whereas for $s_3 > 0$ the variable s_3 increases and σ_3 decreases (see Figure 11).

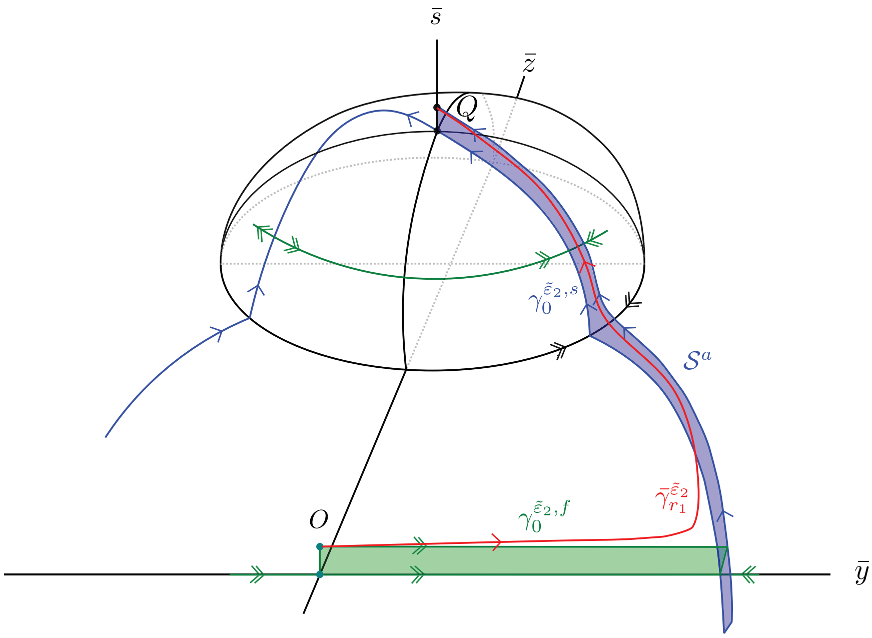

FIGURE 11 | Dynamics of the blown-up extended system (4.21).

For the remaining analysis of $\mathcal{S}^a$ close to the top of the sphere, we change to the scaling chart $\mathcal{K}_{12}^3$ where the dynamics is governed by

$$\begin{aligned} y_2' &= -z_2 - y_2^2 - y_2 c - \sigma_2^2 y_2 z_2 - r_1 y_2 \\ z_2' &= r_1 y_2^2 \\ \sigma_2' &= 0, \end{aligned} \tag{4.28}$$

which is again a slow–fast system with singular perturbation parameter r_1. Note that system (4.28) has a line of equilibria (independent of r_1) at $y_2 = z_2 = 0$ which corresponds to the genuine equilibrium Q.

The layer problem is given by

$$\begin{aligned} y_2' &= -z_2 - y_2^2 - y_2 c - \sigma_2^2 y_2 z_2 \\ z_2' &= 0 \\ \sigma_2' &= 0, \end{aligned} \tag{4.29}$$

with critical manifold

$$\mathcal{S}_2 = \left\{ (y_2, z_2, \sigma_2)^T \in \mathbb{R}^3 : -z_2 - y_2^2 - y_2 c - \sigma_2^2 y_2 z_2 = 0 \right\}. \tag{4.30}$$

For $\sigma_2 = 0$, that is, on the sphere, the critical manifold has the simple form

$$z_2 = -y_2(y_2 + c)$$

with a fold point at $y_2 = -\frac{c}{2}$ and nonvanishing eigenvalue $\lambda = -2y_2 - c$. We conclude that $z_2 = -y_2(y_2 + c)$, $y_2 \geq 0$ is part of the attracting branch $\mathcal{S}_2^a$ of the critical manifold and extends regularly into $\sigma_2 > 0$ since σ_2 is a regular perturbation parameter in (4.30). The critical manifold $\mathcal{S}_2^a$ is uniformly normally attracting for $y \geq 0$ and $\sigma_2 \geq 0$ small enough since for $\sigma_2 = 0$ the fold point at $y_2 = -\frac{c}{2}$ is bounded away from the half space $y_2 \geq 0$. The reduced flow on $\mathcal{S}_2^a$ is given by

$$\dot{z}_2 = y_2^2$$

such that orbits along $\mathcal{S}_2^a$ with $y_2(0) > 0$ converge to the line of equilibria $y_2 = z_2 = 0$ corresponding to Q in a center-like manner, that is, with an algebraic rate. By Fenichel theory, we conclude that there exists a two-dimensional attracting invariant slow manifold $\mathcal{S}_{r_1}^a$ for $0 < r_1 \ll 1$ with slow flow converging to the reduced flow on $\mathcal{S}^a$ as $r_1 \to 0$. Since no new equilibria occur for $r_1 > 0$ all orbits of the slow flow converge to a point on the line of equilibria corresponding to Q. □

Based on Lemma 4.7, we can now construct an $\tilde{\varepsilon}_2$-family of singular orbits connecting the line of initial values corresponding to O with the line of equilibria corresponding Q.

Lemma 4.9. *There exists a family of singular orbits $\gamma_0^{\tilde{\varepsilon}_2}$, $\tilde{\varepsilon}_2 \in [0, 1/\sqrt{\beta_2}]$ of the blown-up extended system of (4.21) connecting the line of initial values with the line of equilibria corresponding to O and Q, respectively.*

Proof. We define the fast fibers connecting the line of initial conditions

$$O_3 = \left(0, \frac{\tilde{\varepsilon}_2}{\sqrt{c}}, \sqrt{c}\right)^T, \ \tilde{\varepsilon}_2 \in [0, 1/\sqrt{\beta_2}]$$

with

$$(y_3, s_3, \sigma_3)^T = \left(1, \frac{\tilde{\varepsilon}_2}{\sqrt{c}}, \sqrt{c}\right)^T \in \mathcal{S}_3^a$$

as $\gamma_0^{\tilde{\varepsilon}_2,f}$. The orbits under the reduced flow along the critical manifold S^a connecting

$$(y_3, s_3, \sigma_3)^T = \left(1, \frac{\tilde{\varepsilon}_2}{\sqrt{c}}, \sqrt{c}\right)^T \in S_3^a$$

with the line of equilibria

$$Q_2 = (0, 0, \tilde{\varepsilon}_2)^T \in \mathbb{R}^3 : \tilde{\varepsilon}_2 \in [0, 1/\sqrt{\beta_2}]\}$$

are defined as $\gamma_0^{\tilde{\varepsilon}_2,s}$

The $\tilde{\varepsilon}_2$-family of singular orbits is therefore given by

$$\gamma_0^{\tilde{\varepsilon}_2} := \gamma_0^{\tilde{\varepsilon}_2,f} \cup \gamma_0^{\tilde{\varepsilon}_2,s},$$

see Figure 11. □

In the following result, we prove that the singular orbits $\gamma_0^{\tilde{\varepsilon}_2}$ perturb to smooth orbits connecting O and Q for $0 < r_1 \ll 1$.

Theorem 4.10. *There exists a constant $\tilde{r} > 0$ such that for all $\tilde{\varepsilon}_2 \in (0, 1/\sqrt{\beta_2}]$ and $r_1 \in (0, \tilde{r}]$, there exists a smooth orbit $\gamma_{r_1}^{\tilde{\varepsilon}_2}$ of (4.21) connecting the initial value O with the genuine equilibrium Q. The corresponding orbit in blown-up space $\bar{\gamma}_{r_1}^{\tilde{\varepsilon}_2}$ is $\mathcal{O}(r_1)$-close to its corresponding singular orbit $\gamma_0^{\tilde{\varepsilon}_2}$ in Hausdorff distance.*

Proof. The existence of the singular orbits in Lemma 4.9, standard Fenichel theory, Lemma 4.7, and arguments similar to the proof of Theorem 3.2 imply that the forward solution with initial value O converges to Q for $0 < r_1 \ll 1$. We denote this solution by $\bar{\gamma}_{r_1}^{\tilde{\varepsilon}_2}$ which by construction is $\mathcal{O}(r_1)$-close to the singular orbit $\bar{\gamma}_0^{\tilde{\varepsilon}_2}$ for all $\tilde{\varepsilon}_2 \in (0, 1/\sqrt{\beta_2}]$ and $0 < r_1 \ll 1$. The assertions of the theorem follow by applying the blowup transformation (4.7), that is, $\gamma_{r_1}^{\tilde{\varepsilon}_2} = \Phi(\bar{\gamma}_{r_1}^{\tilde{\varepsilon}_2})$. □

Remark 4.11. Note that $\tilde{\varepsilon}_2 = 0$ is not included in Theorem 4.10, since this corresponds to the original parameters $\varepsilon_1 = \varepsilon_2 = 0$. In this case, we do not observe dynamics because $y = 0$ is a line of equilibria, as already mentioned in the rough classification in the beginning of Section 2.

This concludes the analysis in region $\bar{B}_1$. It remains to investigate the dynamics in region $\bar{B}_3$.

5 | Analysis in Region B_3

The analysis in region $\bar{B}_3$ is carried out in chart $\mathcal{P}_2$. Inserting (2.9) into (1.14), we obtain

$$\begin{aligned} y' &= r^2\bar{\varepsilon}_1(c - y - z) - y^2 - ryz \\ z' &= y^2. \end{aligned} \tag{5.1}$$

For $r = 0$, this results in the same limiting system as in chart $\mathcal{P}_1$, see (3.2) and Figure 6, with nonhyperbolic critical manifold

$$y = 0.$$

Rescaling y with (3.3), as before, we obtain (after dividing out a factor of r)

$$\begin{aligned} \tilde{y}' &= \bar{\varepsilon}_1(c - r\tilde{y} - z) - \tilde{y}^2 - \tilde{y}z \\ z' &= r\tilde{y}^2. \end{aligned} \tag{5.2}$$

System (5.2) is of standard slow–fast type with singular perturbation parameter r. In the following, we will again omit the "~".

The corresponding layer problem is given by

$$\begin{aligned} y' &= \varepsilon_1(c - z) - y^2 - yz \\ z' &= 0, \end{aligned} \tag{5.3}$$

which for $\varepsilon_1 > 0$, resembles (actually is identical to) the situation in region $\bar{B}_2$. Indeed, the critical manifold is given by

$$S = \left\{(y, z)^T \in \mathbb{R}^2 : \varepsilon_1(c - z) - y^2 - yz = 0\right\} \tag{5.4}$$

and is normally attracting (repelling) for all $y > -\varepsilon_1$ $(y < -\varepsilon_1)$) (see Figure 12a and compare with Figure 7c).

In the limit $\varepsilon_1 \to 0$, normal hyperbolicity is lost at the origin since for $\varepsilon_1 = 0$ the critical manifold consists of two lines

$$y = 0 \text{ and } z = -y$$

which intersect at the origin. The linearization of the layer problem (5.3) at these lines has eigenvalue $\lambda_1 = -z$ and $\lambda_2 = -y$, respectively. Hence, the critical manifold S is not normally hyperbolic at the origin for $\varepsilon_1 = 0$ (see Figure 12b).

To regain normal hyperbolicity, we once again enlarge phase space by adding the equation $\varepsilon_1' = 0$ and blow up the degenerate equilibrium $(y, z, \varepsilon_1)^T = (0, 0, 0)^T$ of this extended system. The suitable blowup transformation is

$$\Phi : [0, \infty) \times \mathbb{S}^2 \to \mathbb{R}^3$$
$$(\sigma, \bar{y}, \bar{z}, \bar{\varepsilon}_1) \mapsto \begin{cases} y = \sigma\bar{y} \\ z = \sigma\bar{z} \\ \varepsilon_1 = \sigma^2\bar{\varepsilon}_1, \end{cases} \tag{5.5}$$

which uses the same weights as the analysis of the slow passage through a transcritical bifurcation, see [25].

Lemma 5.1. *In the blown-up space of system (5.2) extended by the equation $\varepsilon_1' = 0$, there exists for $r = 0$ a two-dimensional attracting critical manifold S^a (shown blue in Figure 13), which contains the line of equilibria corresponding to the genuine equilibrium Q. The critical manifold S^a perturbs regularly to a slow manifold S_r^a for $r > 0$ small enough. All orbits of the reduced flow on S^a approach the line of equilibria in the center direction, that is, with an algebraic rate, for all $0 < \varepsilon_1 \leq \beta_3$.*

Remark 5.2. For better visibility, we have changed the orientation in Figure 13, that is, we look toward the origin from the $\bar{z} = 1$ side of the sphere.

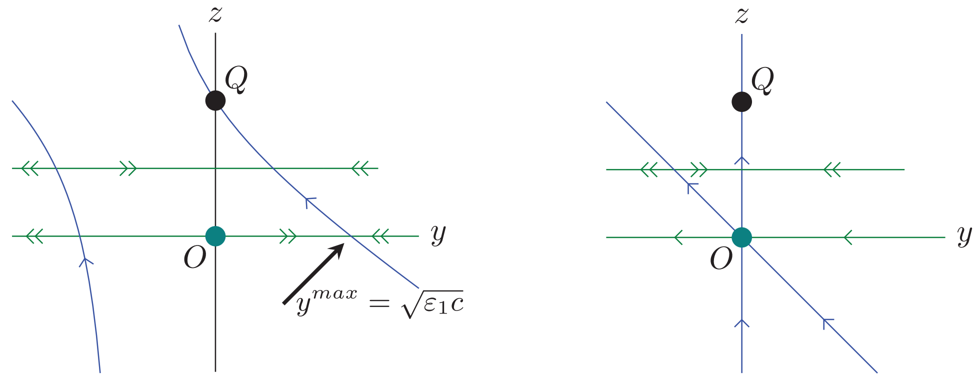

(a) $0 < \varepsilon_1 < c$. (b) $\varepsilon_1 = 0$.

FIGURE 12 | Singular dynamics of (5.2).

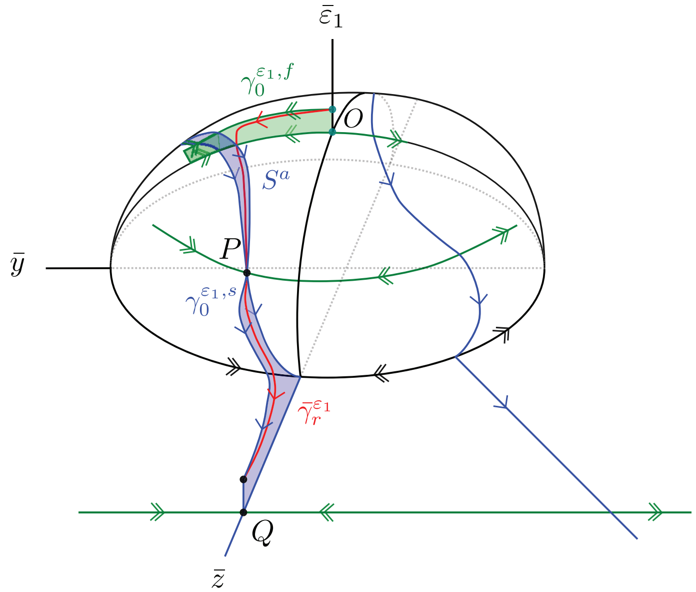

FIGURE 13 | Dynamics of the blown-up extended system (5.2).

Proof. Again, it will be convenient to work in directional charts, which we denote by $\mathcal{K}_3^2$ and $\mathcal{K}_3^3$. The blowup transformation in these charts is given by

$$\mathcal{K}_3^2 : y = \sigma_2 y_2, \quad z = \sigma_2 z_2, \quad \varepsilon_1 = \sigma_2^2 \tag{5.6}$$

$$\mathcal{K}_3^3 : y = \sigma_3 y_3, \quad z = \sigma_3, \quad \varepsilon_1 = \sigma_3^2 \varepsilon_{13}, \tag{5.7}$$

covering the top $\bar{\varepsilon}_1 > 0$ and the front $\bar{z} > 0$ part of the sphere, respectively (see Figure 13). The parts of S^a investigated in chart $\mathcal{K}_3^2$ and $\mathcal{K}_3^3$ are denoted by S_2^a and S_3^a, respectively. Since we have blown-up the initial value O, we start the analysis in the scaling chart $\mathcal{K}_3^2$, where the dynamics is governed by

$$\begin{aligned} y_2' &= c - \sigma_2 z_2 - y_2^2 - y_2 z_2 - r\sigma_2 y_2 \\ z_2' &= r y_2^2 \\ \sigma_2' &= 0. \end{aligned} \tag{5.8}$$

System (5.8) is of standard slow–fast type with singular perturbation parameter r. The corresponding layer problem is given by

$$\begin{aligned} y_2' &= c - \sigma_2 z_2 - y_2^2 - y_2 z_2 \\ z_2' &= 0 \\ \sigma_2' &= 0. \end{aligned} \tag{5.9}$$

For $r = 0$, we find the critical manifold

$$\mathcal{S}_2 = \left\{ (y_2, z_2, \sigma_2)^T \in \mathbb{R}^3 : c - \sigma_2 z_2 - y_2^2 - y_2 z_2 = 0 \right\}, \tag{5.10}$$

which simplifies on the sphere $\sigma_2 = 0$ to $z_2 = \frac{c}{y_2} - y_2$.

As already indicated in Remark 4.8, we note the following.

Remark 5.3. In system (5.8), r is the slow–fast parameter and σ_2 changes the geometry of the critical manifold. Translated to the original parameters, that is, undoing the blowup transformations (2.9) and (5.6), this implies that in region B_3 we have

ε_2 as slow–fast parameter and ε_1 changes the geometry of the critical manifold.

The eigenvalue of the linearization of the layer problem (5.9) is $\lambda = -2y_2 - z_2$. We conclude that the curve $z_2 = \frac{c}{y_2} - y_2$, $y_2 > 0$ on the sphere $\sigma_2 = 0$ is part of the normally attracting branch of the critical manifold $\mathcal{S}_2^a$, which again extends regularly into $\sigma_2 > 0$, since σ_2 acts as a regular perturbation parameter in (5.10).

The reduced flow on S_2^a is given by

$$\dot{z}_2 = y_2^2,$$

hence z_2 increases for all $y_2 \neq 0$ (see Figure 13).

For the remaining analysis of $\mathcal{S}^a$ away from the sphere, we change to the exit chart $\mathcal{K}_3^3$ where the dynamics is governed by

$$\begin{aligned} y_3' &= \varepsilon_{13}(c - r\sigma_3 y_3 - \sigma_3) - y_3^2 - y_3 - r y_3^3 \\ \sigma_3' &= r\sigma_3 y_3^2 \\ \varepsilon_{13}' &= -2r\varepsilon_{13} y_3^2. \end{aligned} \tag{5.11}$$

The layer problem is now given by

$$\begin{aligned} y_3' &= \varepsilon_{13}(c - \sigma_3) - y_3^2 - y_3 \\ \sigma_3' &= 0 \\ \varepsilon_{13}' &= 0, \end{aligned} \tag{5.12}$$

with critical manifold

$$\mathcal{S}_3 = \left\{ (y_3, \sigma_3, \varepsilon_{13})^T \in \mathbb{R}^3 \,:\, \varepsilon_{13}(c - \sigma_3) - y_3^2 - y_3 = 0 \right\}. \tag{5.13}$$

On the invariant plane $\varepsilon_{13} = 0$, the critical manifold $\mathcal{S}_3$ corresponds to the lines $y_3 = 0$ and $y_3 = -1$. The eigenvalue of the linearization of the layer problem (5.12) is $\lambda = -2y_3 - 1$, hence the line $y_3 = 0$, $\varepsilon_{13} = 0$ is part of the normally attracting branch S_3^a of the critical manifold. As before this line extends regularly into $\varepsilon_{13} > 0$ to a smooth manifold $\mathcal{S}_3^a$.

The reduced flow on S_3^a is given by

$$\begin{aligned} \sigma_3' &= \sigma_3 y_3^2 \\ \varepsilon_{13}' &= -2\varepsilon_{13} y_3^2, \end{aligned} \tag{5.14}$$

such that σ_3 increases and ε_{13} decreases for $y_3 > 0$ on $\mathcal{S}_3^a$. All orbits on S_3^a with σ_3, $\varepsilon_{13} > 0$ approach the line of equilibria $y_3 = 0, \sigma_3 = \sqrt{c}$ corresponding to Q (which is contained in $\mathcal{S}_3^a$) in a center-like manner, that is, with an algebraic rate. For completeness, note that on the invariant plane $\varepsilon_{13} = 0$ the critical manifold corresponds to the line $y_3 = 0$ with stationary reduced flow. We conclude that there exists a two-dimensional attracting invariant slow manifold $\mathcal{S}_r^a$ for $0 < r \ll 1$ with slow flow converging to the reduced flow on $\mathcal{S}^a$ as $r \to 0$. Since no new equilibria occur for $r > 0$, all orbits of the slow flow converge to a point on the line of equilibria corresponding to Q. $\square$

Based on Lemma 5.1, we can now construct an ε_1-family of singular orbits connecting the line of initial values corresponding to O with the line of equilibria corresponding to Q.

Lemma 5.4. *There exists a family of singular orbits $\gamma_0^{\varepsilon_1}$, $\varepsilon_1 \in [0, \beta_3]$ of the blown-up extended system of (5.2) connecting the line of initial values with the line of equilibria corresponding to O and Q, respectively.*

Proof. We define the fast fibers connecting the line of initial conditions

$$O_2 = (0, 0, \sqrt{\varepsilon_1})^T, \ \varepsilon_1 \in [0, \beta_3]$$

with

$$(y_2, z_2, \sigma_2)^T = (\sqrt{c}, 0, \sqrt{\varepsilon_1})^T \in S_2^a$$

as $\gamma_0^{\varepsilon_1, f}$. The forward orbits under the reduced flow along the critical manifold $\mathcal{S}^a$ connecting

$$(y_2, z_2, \sigma_2)^T = (\sqrt{c}, 0, \sqrt{\varepsilon_1})^T \in S_2^a$$

with the line of equilibria

$$Q_3 = \left(0, c, \frac{\varepsilon_1}{c^2}\right)^T \in S_3^a, \ \varepsilon_1 \in [0, \beta_3]$$

are denoted as $\gamma_0^{\varepsilon_1, s}$. The ε_1-family of singular orbits is therefore given by

$$\gamma_0^{\varepsilon_1} := \gamma_0^{\varepsilon_1, f} \cup \gamma_0^{\varepsilon_1, s},$$

see Figure 13. $\square$

The following theorem assures that the singular orbits $\gamma_0^{\varepsilon_1}$ perturb to smooth orbits connecting O and Q for $0 < r \ll 1$.

Theorem 5.5. *There exists a constant $r_0 > 0$ such that for all $\varepsilon_1 \in (0, \beta_3]$ and $r \in (0, r_0]$, there exists a smooth orbit $\gamma_r^{\varepsilon_1}$ of (5.2) connecting the initial value O with the genuine equilibrium Q. The corresponding orbit in blown-up space $\bar{\gamma}_r^{\varepsilon_1}$ is $\mathcal{O}(r)$-close to its corresponding singular orbit $\gamma_0^{\varepsilon_1}$ in Hausdorff distance.*

Proof. Combining Lemmas 5.1 and 5.4, it follows from standard Fenichel theory with slow–fast parameter r applied to the blown-up extended system of (5.2) and arguments similar to the proof of Theorem 3.2 imply that the singular orbits $\gamma_0^{\varepsilon_1}$ perturb to smooth orbits $\bar{\gamma}_r^{\varepsilon_1}$ converging to Q, which are $\mathcal{O}(r)$-close for all $\varepsilon_1 \in (0, \varepsilon_3]$ and $r > 0$ small enough. The assertions of the theorem follow by applying the blowup map (5.5), that is, $\gamma_r^{\varepsilon_1} = \Phi(\bar{\gamma}_r^{\varepsilon_1})$. $\square$

Remark 5.6. Note that $\varepsilon_1 = 0$ (actually $\tilde{\varepsilon}_1 = 0$ since the theorem is stated in chart $\mathcal{P}_2$) is not included in Theorem 5.5, since this corresponds to the original parameter $\varepsilon_1 = 0$. In this case, we do not observe dynamics because $y = 0$ is a line of equilibria, as already mentioned in the rough classification in the beginning of Section 2.

We conclude with the proof of the main result, that is, Theorem 1.5.

Proof of Theorem 1.5. It follows from Theorems 3.2, 4.6, 4.10, and 5.5 that in each of the regions B_{11}, B_{12}, B_2, and B_3 there exists a different slow–fast structure of (1.14) with a corresponding singular orbit γ_0 which perturbs to a genuine orbit for $\varepsilon_1, \varepsilon_2$

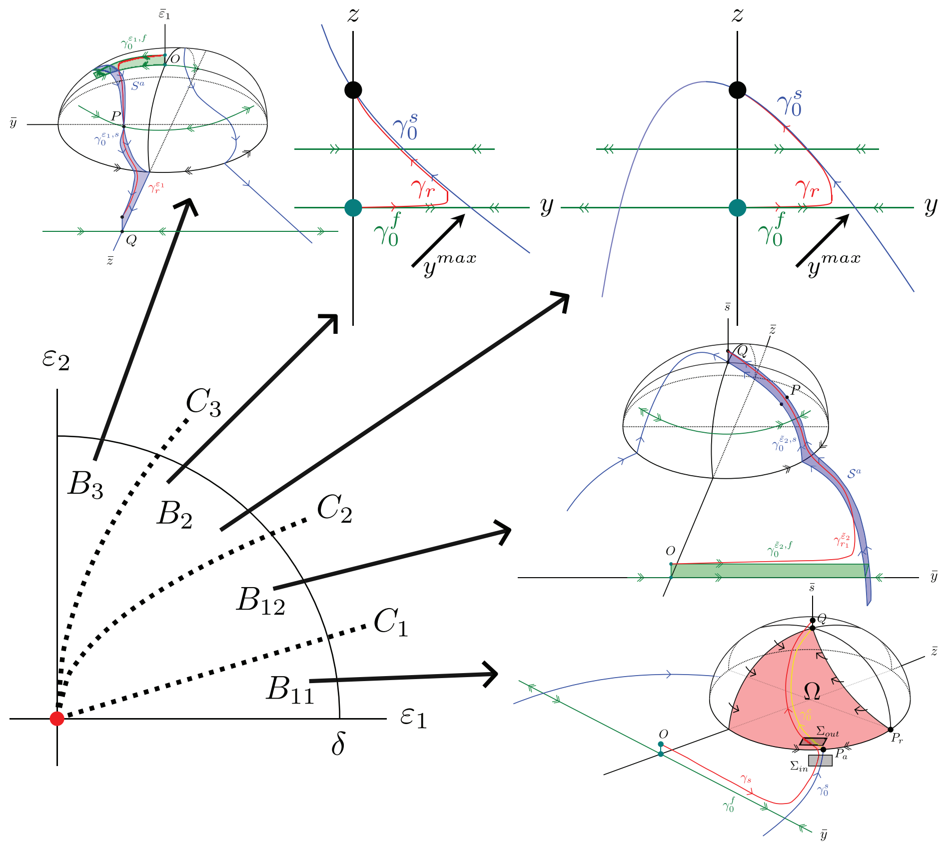

FIGURE 14 | Multiscale structure and singular orbits of (1.14) in different regions of parameter space.

small. The error estimates in ε_1 and ε_2 for each case are obtained by undoing the rescalings of the blowup transformations as in (3.12). □

6 | Summary and Outlook

In this paper, we conducted an asymptotic analysis of the Robertson model, a prominent example of stiffness in ODEs characterized by three reaction rates k_1, k_2, and k_3 of widely differing orders of magnitude. We focused on the scenario where $k_1, k_3 \ll k_2$. By rescaling the problem in terms of the small parameters $(\varepsilon_1, \varepsilon_2) := (k_1/k_2, k_3/k_2)$, we transformed the original equations into a two-parameter singular perturbation problem. To deal with the singular structures associated with the two small parameters, we introduced suitable blowup transformations in parameter space. This allowed us to systematically explore the behavior of the system in a neighborhood of the singular limit $(\varepsilon_1, \varepsilon_2) = (0, 0)$. Our analysis revealed four distinct scaling regimes with different singular structures. Within each regime, we applied GSPT and further blowups in phase space to investigate the dynamics and the structure of the solutions. This combined approach enabled us to capture the various multiscale structures of the model, see Figure 14, which illustrates the main result Theorem 1.5 and the details of the analysis given in Sections 3, 4, and 5. In each region, we identified a specific type of singular orbit connecting the initial value O with equilibrium Q, which perturbs to a genuine orbit (shown in red) for $\varepsilon_1, \varepsilon_2$ small.

TABLE 1 | Comparison of the numerical (y^{max}_{num}) and the analytical (y^{max}) plateau value obtained at representative points $(\varepsilon_1, \varepsilon_2)$ in the different parameter regions corresponding to the simulations shown in Figure 4.

Region	$y^{\max}_{\text{num}}$	$y^{\max}$
B_{11}	$2.16 \cdot 10^{-2}$	$2.2 \cdot 10^{-2} + \mathcal{O}(10^{-4})$
B_{12}	$6.98 \cdot 10^{-3}$	$7.0 \cdot 10^{-3} + \mathcal{O}(10^{-5})$
B_2 (lower)	$7.05 \cdot 10^{-4}$	$7.07 \cdot 10^{-4} + \mathcal{O}(10^{-7})$
B_2 (upper)	$7.07 \cdot 10^{-5}$	$7.071 \cdot 10^{-5} + \mathcal{O}(10^{-9})$
B_3	$2.26 \cdot 10^{-6}$	$2.236 \cdot 10^{-6} + \mathcal{O}(10^{-10})$

The asymptotic results derived from our analysis are in excellent qualitative and quantitative agreement with numerical simulations, compare Figure 4 with 14, for example, the maximal value of the y-component. Our analysis predicts $y^{max} = \sqrt{\varepsilon_1 c} + \mathcal{O}(\varepsilon_1)$ in B_{11}, B_{12}, and B_2 and $y^{max} = \sqrt{\varepsilon_1 c} + \mathcal{O}(\sqrt{\varepsilon_1}\varepsilon_2)$ in B_3. The values obtained for y^{max} (with the same parameter values as in the simulations shown in Figure 4) are collected in Table 1, which fit well with the corresponding numerical results y^{max}_{num} of the simulations shown in Figure 4. In addition, we observe in Figure 4 that the time it takes for z to increase becomes longer as we move counterclockwise. The analytical explanation for this observation is the change in the geometry of the attracting part of the critical manifold S^a in the different regions (cf., Figure 14).

Overall, this work provides a thorough understanding of the dynamics and detailed asymptotics of the Robertson model.

This case study highlights the potential of combining GSPT with blowup in parameter space for analyzing multiparameter singular perturbation problems. We believe that this approach is applicable to more complicated problems and has the potential to lead to a framework for the analysis of multiparameter singular perturbations. In ongoing work, we are using this approach in the analysis of a five-variable model of the cell cycle [8, 36] with singular dependence on three parameters.

Acknowledgments

We thank two anonymous referees for their helpful suggestions. The authors acknowledge TU Wien Bibliothek for financial support through its Open Access Funding Programme.

Data Availability Statement

Data sharing not applicable to this article as no data sets were generated or analyzed during the current study.

References

1. H. Amann, *An Introduction to Nonlinear Analysis* (De Gruyter, 1990).

2. L. Baumgartner, "Geometric Analysis of Multi-Parameter Singular Perturbation Problems" (PhD thesis, TU Wien, ongoing).

3. A. Bruno, *Power Geometry in Algebraic and Differential Equations*, North-Holland Mathematical Library (Elsevier Science, 2000).

4. P. T. Cardin and M. A. Teixeira, "Fenichel Theory for Multiple Time Scale Singular Perturbation Problems," *SIAM Journal on Applied Dynamical Systems* 16, no. 3 (2017): 1425–1452.

5. P. Carter, A. Doelman, A. Iuorio, and F. Veerman, "Travelling Pulses on Three Spatial Scales in a Klausmeier-Type Vegetation-Autotoxicity Model," *Nonlinearity* 37, no. 9 (2024): 095008.

6. P. De Maesschalck and F. Dumortier, "Canard Cycles in the Presence of Slow Dynamics With Singularities," *Proceedings of the Royal Society of Edinburgh Section A: Mathematics* 138, no. 2 (2008): 265–299.

7. P. De Maesschalck and F. Dumortier, "Slow-Fast Bogdanov-Takens Bifurcations," *Journal of Differential Equations* 250, no. 2 (2011): 1000–1025.

8. A. Desoeuvres, P. Szmolyan, and O. Radulescu, "Qualitative Dynamics of Chemical Reaction Networks: An Investigation Using Partial Tropical Equilibrations," in *Computational Methods in Systems Biology: 20th International Conference, CMSB 2022, Bucharest, Romania, September 14-16, 2022, Proceedings*, Vol. 13447 (Springer Nature, 2022), 61.

9. F. Dumortier and R. H. Roussarie, *Canard Cycles and Center Manifolds*, American Mathematical Society: Memoirs of the American Mathematical Society (American Mathematical Society, 1996).

10. N. Fenichel, "Geometric Singular Perturbation Theory for Ordinary Differential Equations," *Journal of Differential Equations* 31, no. 1 (1979): 53–98.

11. S. J. Fraser, "Double Perturbation Series in the Differential Equations of Enzyme Kinetics," *Journal of Chemical Physics* 109, no. 2 (1998): 411–423.

12. J. Guckenheimer and P. Holmes, *Nonlinear Oscillations, Dynamical Systems, and Bifurcations of Vector Fields* (Springer, 1983).

13. I. Gucwa and P. Szmolyan, "Geometric Singular Perturbation Analysis of an Autocatalator Model," *Discrete and Continuous Dynamical Systems - S* 2, no. 4 (2009): 783–806.

14. E. Hairer and G. Wanner, *Solving Ordinary Differential Equations II*, 2nd ed. (Springer, 1996).

15. A. Iuorio, N. Popović, and P. Szmolyan, "Singular Perturbation Analysis of a Regularized MEMS Model," *SIAM Journal on Applied Dynamical Systems* 18, no. 2 (2019): 661–708.

16. S. Jelbart, K. U. Kristiansen, P. Szmolyan, and M. Wechselberger, "Singularly Perturbed Oscillators With Exponential Nonlinearities," *Journal of Dynamics and Differential Equations* 122 (2021): 1572–9222.

17. S. Jelbart, C. Kuehn, and S. V. Kuntz, "Geometric Blow-Up for Folded Limit Cycle Manifolds in Three Time-Scale Systems," *Journal of Nonlinear Science* 34, no. 17 (2023): 1432–1467.

18. S. Jelbart, N. Pages, V. Kirk, J. Sneyd, and M. Wechselberger, "Process-Oriented Geometric Singular Perturbation Theory and Calcium Dynamics," *SIAM Journal on Applied Dynamical Systems* 21, no. 2 (2022): 982–1029.

19. C. K. R. T. Jones, "Geometric Singular Perturbation Theory," in *Dynamical Systems*, Lecture Notes in Math., Vol. 1609 (Springer, 1995).

20. I. Kosiuk and P. Szmolyan, "Geometric Analysis of the Goldbeter Minimal Model for the Embryonic Cell Cycle," *Journal of Mathematical Biology* 72, no. 5 (2016): 1337–1368.

21. I. Kosiuk and P. Szmolyan, "Scaling in Singular Perturbation Problems: Blowing Up a Relaxation Oscillator," *SIAM Journal on Applied Dynamical Systems* 10, no. 4 (2011): 1307–1343.

22. N. Kruff, C. Lüders, O. Radulescu, T. Sturm, and S. Walcher, "Algorithmic Reduction of Biological Networks With Multiple Time Scales," *Mathematics in Computer Science* 15 (2021): 499–534.

23. M. Krupa, N. Popović, and N. Kopell, "Mixed-Mode Oscillations in Three Time-Scale Systems: A Prototypical Example," *SIAM Journal on Applied Dynamical Systems* 7, no. 2 (2008): 361–420.

24. M. Krupa and P. Szmolyan, "Extending Geometric Singular Perturbation Theory to Nonhyperbolic Points-Fold and Canard Points in Two Dimensions," *SIAM Journal on Mathematical Analysis* 33, no. 2 (2001): 286–314.

25. M. Krupa and P. Szmolyan, "Extending Slow Manifolds Near Transcritical and Pitchfork Singularities," *Nonlinearity* 14, no. 6 (2001): 1473–1491.

26. M. Krupa and P. Szmolyan, "Relaxation Oscillation and Canard Explosion," *Journal of Differential Equations* 174, no. 2 (2001): 312–368.

27. C. Kuehn, *Multiple Time Scale Dynamics*, Applied Mathematical Sciences, Vol. 191 (Springer, 2015).

28. C. Kuehn, N. Berglund, C. Bick, et al., "A General View on Double Limits in Differential Equations," *Physica D: Nonlinear Phenomena* 431 (2022): 133105.

29. C. Kuehn and P. Szmolyan, "Multiscale Geometry of the Olsen Model and Non-Classical Relaxation Oscillations," *Journal of Nonlinear Science* 25 (2015): 583–629.

30. H. H. Robertson, "The Solution of a Set of Reaction Rate Equations," in *Numerical Analysis: An Introduction* (Academic Press, 1966), 178–182.

31. M. R. Roussel and S. J. Fraser, "Global Analysis of Enzyme Inhibition Kinetics," *Journal of Physical Chemistry* 97, no. 31 (1993): 8316–8327.

32. *SciPy, BDF*, [Online], accessed January 10, 2025, https://docs.scipy.org/doc/scipy/reference/generated/scipy.integrate.BDF.html.

33. L. A. Segel, "On the Validity of the Steady State Assumption of Enzyme Kinetics," *Bulletin of Mathematical Biology* 50, no. 6 (1988): 579–593.

34. T. J. Snowden, P. H. van der Graaf, and M. J. Tindall, "Methods of Model Reduction for Large-Scale Biological Systems: A Survey of Current Methods and Trends," *Bulletin of Mathematical Biology* 79 (2017): 1449–1486.

35. P. Szmolyan and M. Wechselberger, "Canards in $\mathbb{R}^3$," *Journal of Differential Equations* 177 (2001): 419–453.

36. J. J. Tyson, "Modeling the Cell Division Cycle: cdc2 and Cyclin Interactions," *Proceedings of the National Academy of Sciences* 88, no. 16 (1991): 7328–7332.

37. J. J. Tyson, "Scaling and Reducing the Field-Koros-Noyes Mechanism of the Belousov-Zhabotinskii Reaction," *Journal of Physical Chemistry* 86, no. 15 (1982): 3006–3012.

38. M. Wechselberger, *Geometric Singular Perturbation Theory Beyond the Standard Form* (Springer, 2020).